Bona fide hematopoietic stem cells in zebrafish originate from the supra-intestinal artery

Shachuan Feng[1,5], Rui Qu[1,2,5], Yingzhu He[2], Tingting Huang[1], Youqi Wang[1,2], Thi Huong Trinh[1,2], Kefan Cheng[1,2], Shizheng Zhao[1,3], Ying Huang[1,2], Hao Zhu[1,2], Sicong He[1], and Zilong Wen[1,4,*]

[1]Department of Immunology and Microbiology, School of Life Science, Southern University of Science and Technology, Shenzhen 518055, China.

[2]The Hong Kong University of Science and Technology, Clear Water Bay, Hong Kong, China.

[3]Biomedical Research Institute, Shenzhen Peking University—Hong Kong University of Science and Technology Medical Center, Shenzhen 518036, China.

[4]Greater Bay Biomedical Innocenter, Shenzhen Bay Laboratory, Shenzhen 518132, China.

[5]S.F. and R.Q. contribute equally to this work.

*Correspondence should be addressed to ZLW: Department of Immunology and Microbiology, School of Life Science, Southern University of Science and Technology, Shenzhen 518055, China. Tel: (0755)88015676; Email: wenzl@sustech.edu.cn

SUMMARY

Hematopoietic stem cells (HSCs) in vertebrates are widely believed to originate from hemogenic endothelial cells (HECs) in the dorsal aorta (DA) through endothelial-to-hematopoietic transition. However, conclusive in vivo DA-specific lineage-tracing studies to confirm this origin are lacking. Here, leveraging infrared light-mediated temporospatial-resolution lineage-tracing technology, we demonstrate that in zebrafish, HSCs do not originate from the DA. Instead, following the DA hematopoiesis, which produces hematopoietic precursors with limited renewal potential, lifelong renewable HSCs emerge from the supra-intestinal artery (SIA). Remarkably, while the DA produces hematopoietic cells from unipotent HECs, the SIA generates hematopoietic cells from both unipotent HECs and bipotent vessel-resident hemangioblasts (VRHs). These VRHs undergo multiple rounds of division and budding, generating both hematopoietic cells and SIA-resident endothelial cells. The distinct characteristics of DA and SIA cells are further reinforced by single-cell transcriptomic profiling. Our findings challenge the current paradigm of HSC development, underscoring the complexity of vertebrate hematopoiesis.

INTRODUCTION

In vertebrates, most mature blood cells have short lifespans and must be continuously replenished by hematopoietic stem cells (HSCs), which possess the unique ability to self-renew and differentiate into all blood lineages throughout an organism' s lifespan.[1] The development, maintenance, and differentiation of HSCs are governed by tightly regulated processes, and disruptions to these mechanisms are frequently linked to the pathogenesis of diverse diseases, including cancers.[2,3] The importance of HSCs is further exemplified by their pivotal role in modern medical interventions, as HSC transplantation has emerged as a highly effective therapy for a wide array of severe blood disorders.[4,5] Hence, elucidating the cellular and molecular mechanisms underlying HSC establishment and maintenance holds promise for advancing novel therapeutic strategies to treat blood-related diseases.

It has been well-accepted that HSCs in vertebrates are generated from the hemogenic endothelial cells (HECs) in the dorsal aorta (DA) through a process called endothelial-to-hematopoietic transitions (EHT).[6-9] This process has been extensively studied and characterized in multiple vertebrate species, especially in mice and zebrafish. The first critical evidence supporting this concept came from the identification of transplantable HSC activity in the aorta-gonad-mesonephros (AGM) region of mouse embryos at embryonic day 9.5-10 (E9.5-10), as well as in ex vivo cultured AGM explants.[10-12] These findings suggest that the AGM serves as the primary site of HSC generation in mice. Similarly, studies in zebrafish have revealed robust hematopoietic activity in the AGM, as evidenced by the strong expression of hematopoietic stem/progenitor cell (HSPC) markers in this region.[13-16] Subsequent in vivo lineage tracing studies conducted in vasculature-specific Cre/CreER^{T2} reporter lines during embryonic stages have demonstrated that labeled cells give rise to various blood lineages that persist into adulthood in both mice and zebrafish,[7,17] pointing to the endothelial origin of HSCs. As the DA is a prominent vascular structure associated with hematopoietic activity in the AGM of both mice and zebrafish,[6,12,18] these studies collectively point to the DA as the principal source of HSC generation. This conclusion

is further reinforced by the detection of hematopoietic cell clusters attached to the DA lumen in E9.5-10.5 mouse embryos and the visualization of EHT in the DA using ex vivo cultured AGM explants and live zebrafish embryos.[6-8,19,20] Perhaps the most compelling evidence arises from the temporospatially controlled lineage-tracing experiments in zebrafish using the infrared light-evoked gene operator (IR-LEGO) system.[21-23] These studies demonstrated that infrared light illumination of the AGM region housing the DA, prior to the onset of EHT, effectively labels multiple blood lineages that persist into adulthood.[21] Collectively, these findings, along with additional supporting studies,[24-27] have established the critical role of the DA in the HSC generation.

Despite these insightful studies, in vivo lineage tracing specifically targeting the DA endothelium to definitively confirm the DA as the primary origin of HSCs has been lacking. Recent research has indicated that lymphoid-biased fetal HSC-like cells, despite not naturally contributing to the adult HSC pool, can be reprogrammed into adult HSCs upon transplantation into irradiated recipient mice.[28] This raises concern about the conclusions drawn from previous transplantation studies regarding the origin of HSCs. Additionally, several studies in mice have indicated the detection of pre-HSCs in the subaortic mesenchyme before the initiation of EHT in the DA, suggesting the possible existence of alternative sources for HSC generation.[29,30] Furthermore, recent findings have revealed that the DA appears to be capable of producing non-HSC hematopoietic progenitors, including embryonic multipotent progenitors in mice and endothelium-derived hematopoietic progenitors (EHPs) in zebrafish,[21,31-34] These discoveries highlight the complexity of hematopoiesis within this vascular structure. Finally, although temporospatially controlled lineage-tracing in zebrafish with the IR-LEGO system has shown that HSCs indeed originate from the AGM region,[21,23] the resolution of the IR-LEGO system employed in these investigations is insufficient to distinguish the DA from other nearby vascular structures within the AGM. Therefore, there is a need for advanced lineage tracing methodologies with enhanced spatial resolution to accurately map the origin of HSCs.

The study described here employed a high-resolution IR-LEGO lineage-tracing system, combined with photoconvertible cell labeling and time-lapse live imaging, to investigate the origin of HSCs in zebrafish. The results reveal that HSCs in zebrafish originate from the supra-intestinal artery (SIA) rather than the DA. In contrast, the DA primarily generates EHPs that do not persist into adulthood. Through in vivo single-cell lineage tracing analysis, we discovered that, unlike the DA, where hematopoietic cells are generated from unipotent HECs, the SIA produces hematopoietic cells through both unipotent HECs and bipotent precursors identified as vessel-resident hemangioblasts (VRHs). These VRHs undergo multiple rounds of division and budding, giving rise to both hematopoietic and endothelial lineages. Finally, single-cell RNA sequencing (scRNA-seq) analysis unveiled distinct transcriptomic profiles and identified unique sets of transcription factors in cells originating from the DA and SIA. These findings reshape the foundations of HSC development studies, highlighting the intricate and multifaceted nature of vertebrate hematopoiesis.

RESULTS

Temporospatially restricted fate mapping challenges the dorsal aorta origin of HSCs

It has been documented that HSCs in vertebrates, including zebrafish, are generated from the HECs in the DA.[35] Surprisingly, recent research has unveiled that zebrafish DA HECs also produce non-HSC hematopoietic progenitors, termed EHPs that are capable of giving rise to various blood lineages during larval and juvenile stages but not in adulthood.[21] This raises questions about the mechanisms underlying the fate specification of HSCs versus EHPs in the DA. To investigate which HECs generate HSCs, we used a single-cell resolution IR-LEGO lineage-tracing system to label individual HECs in the DA and tracked their contribution to adult hematopoietic lineages (Figure 1A).[33] To enhance the efficiency and precision of labeling, we developed a fate mapping line, *Tg(hsp70l:mCherry-T2A-CreER^{T2};kdrl:loxP-DsRedx-loxP-eGFP;coro1a:loxP-DsRedx-loxP-eGFP)* (*loxP-DsRedx-loxP-eGFP* is abbreviated to *LRLG* hereafter), featuring three cassettes: *hsp70l*-CreER^{T2} for infrared light inducible CreER^{T2} expression,[22,36] endothelium-specific *kdrl-LRLG* for targeting DA HECs (*kdrl:*DsRedx^{+}) and identifying embryos with successful labeling of a single HEC (*kdrl:*eGFP^{+}), and hematopoiesis-specific *coro1a-LRLG* for visualizing hematopoietic derivatives (*coro1a:*eGFP^{+}) (Figure 1A).[23,37] Given that HSCs have been shown to originate predominantly from the anterior region of the DA,[21] we focused on the anterior region (between the 8th and 10th somite) of the DA and illuminated a single HEC at 30 hours post-fertilization (hpf), prior to the onset of EHT.[6] 10 hours post-IR illumination, embryos harboring a single *kdrl:*eGFP^{+} HEC in the ventral side of the DA were selected (Figure 1A and 1B) and raised to adulthood for flow cytometry analysis of adult hematopoietic organ—the kidney marrow (KM) (zebrafish counterpart of mammalian bone marrow)[38] (Figures S1A and S1B). Surprisingly, only 4.4% (6 out of 136) of the treated fish exhibited successful labeling of HSCs, as evidenced by the presence of *coro1a:*eGFP^{+} hematopoietic cells encompassing lymphoid, myeloid, and hematopoietic precursor lineages in adult KM (Figures 1C and S1B). This percentage

137 falls significantly below the estimated HSC frequency (~60%, corresponding to ~21
138 HSC precursors and ~34 DA floor HECs)[39,40] and is even lower than the control fish
139 (7.5%, 20/268) (Figure 1C), indicating that the detection of hematopoietic lineages in
140 adult KM in both control and DA-targeted groups is caused by sporadic leaky activity
141 of $CreER^{T2}$. Given that the single cell labeling specifically targeted the anterior DA
142 (between 8th and 10th somite) where HSCs are presumed to be most-enriched,[21] these
143 results suggest that the DA contributes minimally, if at all, to HSC generation.

144 **HSC precursors are spatially restricted to the subaortic AGM region**

145 While previous multi-cell resolution IR-LEGO studies have confirmed HSC emergence
146 from the AGM region,[21,23] our single-cell labeling data suggest that these HSCs likely
147 originate from non-DA tissues within this domain. We thus proposed the subaortic
148 AGM region, where two key components, the gonad and mesonephros of the AGM, are
149 located,[41-43] as the most probable HSC source.

150 To support this speculation, we applied multi-cell resolution IR-LEGO system to
151 label one somite width region between 8th and 10th somite targeting the anterior
152 subaortic AGM region at 28 hpf (Figure 1D) and then tracked their contributions to
153 hematopoietic lineages in adult KM. In parallel, we also targeted the adjacent anterior
154 segment of the DA as the control. The labeling specificity was confirmed by confocal
155 imaging of *kdrl*:eGFP signals in both the subaortic posterior cardinal vein (PCV) and
156 the DA, and embryos with minimal cross-labeling were raised to adulthood for flow
157 cytometry analysis of KM blood cells (Figure 1E). As anticipated, 79% (78 out of 99)
158 of the subaortic AGM region-targeted fish displayed abundant *coro1a:*$eGFP^+$
159 hematopoietic cells, encompassing lymphoid, myeloid, and hematopoietic precursor
160 lineages, in adult KM (Figures 1F and S1C). In contrast, only 16% (14 out of 85) of the
161 DA region-targeted fish showed coro1a:eGFP+ hematopoietic cells in adult KM
162 (Figures 1F and S1C), a moderate increase compared to the untargeted fish (2.7%, 3
163 out of 110). More importantly, an average of 12.8% of adult KM HSCs were labeled in
164 the subaortic AGM region-targeted fish, a striking contrast to 1.35% in the DA region-
165 targeted fish and 0.23% in control fish (Figure 1G). The minimal labeling percentage

166 of hematopoietic cells in the DA region-targeted fish suggests that the observed HSC
167 labeling in this group is most likely due to sporadic CreER^{T2} leaky activity and
168 unavoidable occasional cross-labeling of the subaortic AGM region by multi-cell
169 resolution IR illumination. Collectively, these results, combined with single-cell fate
170 mapping data, suggest that the majority of HSCs do not originate from the DA but
171 instead arise from precursor cells residing in the subaortic AGM region.

172 **HSCs arise from previously unidentified precursors located beneath the anterior**
173 **region of the PCV**

174 Previous studies in both mammals and zebrafish have supported the endothelial origin
175 of HSCs.[21,23] As PCV is the major vasculature in the subaortic AGM region,[44] we
176 hypothesized that PCV might be the source giving rise to HSCs. We therefore
177 performed time-lapse live imaging on venous endothelium reporter line
178 *Tg(stab1:DsRedx)* to determine whether EHT occurs in the PCV. Surprisingly, no EHT
179 was observed during the imaging period spanning from 29 hpf to 72 hpf (Figure 2A;
180 Movie S1), indicating that HSCs are unlikely to originate directly from the PCV. To
181 reinforce this notion, we crossed the lymphatic/venous endothelium-specific CreER^{T2}
182 line *Tg(lyve1b:CreER^{T2})*[45] with the *Tg(kdrl:LRLG;coro1a:LRLG)* reporter line to
183 generate triple transgenic fish for fate mapping analysis (Figure 2B). As predicted,
184 despite effectively labeling nearly all PCV endothelial cells (Figure 2B), only 8% (6
185 out of 71) of the fish showed limited *coro1a*:eGFP^{+} hematopoietic cells in adult KM,
186 with an average HSC-labeling efficiency of only 0.61% (Figures 2C and 2D). In
187 contrast, all pan-endothelial *Tg(kdrl:CreER^{T2})* fish (15 out of 15) exhibited robust HSC-
188 labeling, with an average HSC-labeling efficiency of 66.97% (Figures 2C, 2D, and
189 S2A). These findings, combined with time-lapse live imaging data, confirm that HSCs
190 do not originate from the PCV but most likely arise from undisclosed *kdrl*-positive
191 precursors situated in the vicinity of the anterior PCV.

192 To further identify the precise location of these undisclosed precursors, we applied
193 the IR-LEGO lineage-tracing system to target either the dorsal or ventral side of the
194 anterior PCV in the *Tg(hsp70l:mCherry-T2A-CreER^{T2};kdrl:LRLG;coro1a:LRLG)*

195 reporter line and assessed HSC-labeling frequency in each group (Figures 2E and S2B).
196 The results showed that ~70% of the fish targeted on the ventral side contained
197 abundant *coro1a:*eGFP^{+} hematopoietic cells in adult KM, compared to only 34% in the
198 dorsal-targeted group (Figure 2F). Together, these findings indicate that the majority of
199 undisclosed HSC precursors are located beneath the anterior PCV.

200 **The supra-intestinal artery gives rise to HSCs via EHT**

201 Given the fact that most adult zebrafish hematopoietic cells are likely of endothelial
202 origin,[7] we hypothesized that HSCs are probably derived from a subset of endothelial
203 precursors positioned beneath the anterior PCV. Notably, three vascular structures are
204 known to develop beneath the PCV during zebrafish embryogenesis: the supra-
205 intestinal artery (SIA), sub-intestinal vein (SIV), and sub-intestinal venous plexus
206 (SIVP).[44,46-49] We reasoned that one or more of these vascular structures might serve as
207 the source of HSCs. To test this, we examined these vessels from 2 days post
208 fertilization (dpf) to 7 dpf, after the SIA, SIV, and SIVP are well-established, for
209 potential budding cells. Confocal imaging in *Tg(fli1:eGFP)* fish did not capture any
210 potential budding cells before 4 dpf (Figure S3A), but by 7 dpf, a few potential budding
211 cells were detected in the anterior SIA but not in the SIV and SIVP (Figure S3B). This
212 suggests that the SIA may be the source generating HSCs from 4 dpf onwards. To
213 support this speculation, we conducted time-lapse live imaging using the *Tg(kdrl:eGFP)*
214 reporter line from 4 dpf onwards. Remarkably, we found that the endothelium in the
215 anterior SIA, but not in the posterior SIA, the SIV, and the SIVP, undergoes EHT,
216 producing cells resembling hematopoietic cells (Figure 3A; Movie S2). To verify that
217 SIA-derived cells are indeed hematopoietic cells, we photoconverted the anterior SIA
218 in 4 dpf *Tg(kdrl:Dendra2)* larvae and tracked the fates of the converted cells at later
219 stages. The results showed that the photoconverted Dendra2-red cells were increasingly
220 detected in the thymus and caudal hematopoietic tissue (CHT), two well-known
221 hematopoietic tissues in zebrafish,[50,51] from 5 dpf to 7 dpf, documenting their
222 hematopoietic identity (Figures 3B, 3C, and S3C).

223 To confirm the presence of HSCs among SIA-derived hematopoietic cells, we

224 employed muti-cell resolution IR-LEGO system to permanently label the anterior SIA
225 region in the *Tg(hsp70l:mCherry-T2A-CreER^{T2};kdrl:LRLG;coro1a:LRLG)* reporter
226 line at 5 dpf, a stage where the anterior SIA is well-separated from the PCV by the
227 swimming bladder (Figure 3D).[52] The anterior PCV region was also labeled as a control.
228 The infrared light labeling of the SIA and PCV was highly specific, with no cross-
229 labeling observed (Figure 3E). The IR-illuminated fish were raised to adulthood and
230 analyzed by flow cytometry for adult KM (Figure S3D). Consistent with our hypothesis,
231 85% of SIA region-targeted fish exhibited abundant *coro1a:*eGFP^{+} hematopoietic cells
232 (lymphoid, myeloid, and precursor lineages), while these cells were absent in the PCV
233 region-targeted group (Figure 3F). Among the SIA region-targeted fish with
234 successfully labeled adult blood cells, ~20% of all three major cell populations were
235 labeled on average, with the highest labeling efficiency reaching ~60% (Figure 3G).
236 Collectively, these findings, combined with time-lapse live imaging and
237 photoconversion assays, demonstrate that the majority of HSCs are generated from the
238 anterior SIA through EHT.

239 **HSC emergence from the supra-intestinal artery requires Runx1 and Notch**
240 **signaling**

241 The transcription factor RUNX1/Runx1 is known to play a crucial role in EHT in the
242 DA of both mammals and zebrafish.[6,53] We thus hypothesized that Runx1 also regulates
243 EHT in the SIA. To test this, we crossed *runx1*-deficient *runx1^{w84x}* mutants with the
244 *Tg(kdrl:eGFP)* reporter line and quantified SIA-associated *kdrl:*eGFP^{+} cells,[54,55] which
245 likely represent nascent HSCs derived from the SIA (Figure 4A and 4B). As expected,
246 *runx1^{w84x}* mutants showed a significant reduction in SIA-associated *kdrl:*eGFP^{+} cells
247 (Figure 4B), indicating that *runx1* deficiency disrupts the formation of SIA-born HSCs.
248 To confirm this was due to EHT defects, we performed time-lapse live imaging on 4-6
249 dpf *Tg(kdrl:eGFP);runx1^{w84x}* mutant larvae. Consistent with our hypothesis, EHT in
250 the SIA was nearly absent in the mutants (Movie S3). Collectively, these findings
251 demonstrate that, similar to the DA,[6] *runx1* is essential for hematopoietic cell
252 generation in the SIA.

253 Previous studies have established the critical role of Notch signaling in HSPC
254 formation in both mammals and zebrafish.[56-58] However, the conclusions in zebrafish
255 primarily rely on detecting *runx1*$^{+}$ HECs in the DA and *runx1*$^{+}$/*cmyb*$^{+}$/*cd41*$^{+}$
256 hematopoietic cells in the AGM region.[57,59] which, as our fate-mapping study shows,
257 are largely EHPs derived from the DA (Figures 1C, 1F, and 1G). Thus, it is essential to
258 reassess the role of Notch signaling in the development of bona fide HSCs originating
259 from the SIA. To address this, we treated the *Tg(kdrl:eGFP)* embryos with the Notch
260 inhibitor DAPT[60] from 2.5 dpf to 4.5 dpf, shortly after SIA formation,[46] and evaluated
261 its impact on SIA hematopoiesis by quantifying SIA-associated *kdrl:*eGFP^{+} HSPC-like
262 cells a few days later. Indeed, DAPT treatment significantly reduced SIA-associated
263 *kdrl:*eGFP^{+} cells (Figures 4C and 4D), underscoring the pivotal role of Notch signaling
264 in SIA hematopoiesis. To pinpoint the stage at which Notch signaling acts, we
265 administered DAPT treatment to embryos during two windows: 2.5-3.5 dpf (prior to
266 EHT initiation) and 3.5-4.5 dpf (after EHT initiation). Only the treatment during 2.5-
267 3.5 dpf significantly reduced SIA-associated *kdrl:*eGFP^{+} cells (Figures 4C and 4D).
268 suggesting Notch signaling regulates SIA hematopoiesis before EHT initiation, likely
269 by influencing the formation of the HECs. To validate this, we performed RNAscope
270 in situ hybridization of *gata2b*, a well-known regulator of HEC fate,[61] in DAPT- and
271 DMSO-treated 5 dpf *Tg(kdrl:eGFP)* fish. As anticipated, *gata2b* was robustly
272 expressed in the majority of anterior SIA cells in the DMSO-treated fish but largely
273 absent in SIA in DAPT-treated fish (Figure 4E), consistent with the role of Notch
274 signaling in HEC formation in the DA.[40,57,62] Notably, in DMSO-treated fish, the
275 majority of anterior SIA cells exhibited *gata2b* expression, further supporting the idea
276 that the SIA lacks the dorsal-ventral polarity and that most, if not all, anterior SIA cells
277 possess hemogenic potential.

278 **Supra-intestinal artery hematopoiesis involves vessel-resident hemangioblasts and**
279 **sustains an extended period**

280 To unveil the dynamics of HSC generation in the SIA, we leveraged the *Tg(kdrl:eGFP)*
281 reporter line to quantify eGFP^{+} cells closely associated with the SIA, which likely

represent nascent HSCs derived from the SIA, starting at 5 dpf (Figure 5A). We found that SIA-associated eGFP$^+$ cells were consistently detected at 5 dpf, increased steadily to a peak of ~15 cells by 7-8 dpf, and then gradually declined from 10 dpf onwards, remaining detectable until 15 dpf (Figure 5B).

Since the number of SIA-associated eGFP$^+$ cells reflects a combination of EHT along with the proliferation and migration rates of these cells, it may not accurately represent the true dynamics of SIA hematopoiesis. To better elucidate these dynamics, we utilized endothelium-specific *Tg(kdrl:Dendra2)* transgenic fish[21,63] and photoconverted single HECs/ECs in the anterior SIA from 3 dpf to 16 dpf. 24 hours post-photoconversion, we assessed the EHT frequency by calculating the ratio of fish with SIA-associated Dendra2-Red cells, presumably representing the hematopoietic cells derived from converted HECs (Figure 5C). We found that SIA EHT commenced around 4 dpf, with ~17% of converted cells undergoing EHT (Figure 5C). EHT frequency rapidly increased, peaking at ~62% at 4-5 dpf, then gradually declined from 10-11 dpf onwards, stabilizing at a lower level (~27%) until ~17 dpf (Figure 5C). These findings indicate that, unlike the DA where the hematopoiesis initiates early in embryogenesis and diminishes within ~2 days (30-68 hpf),[6] SIA hematopoiesis emerges later during the larval stage and persists for at least two weeks.

Intriguingly, we observed that, in addition to generating hematopoietic progeny via canonical EHT, where photoconverted single cells directly bud out from the SIA (Figure 5D),[40] a subset of converted cells underwent multiple rounds of division and budding, producing both hematopoietic daughter cells and endothelial daughter cells that remained within the SIA (Figure 5D). This prompted us to speculate that these SIA cells are bipotent precursors capable of giving rise to both hematopoietic and endothelial lineages. To support this, we employed the single-cell IR-LEGO lineage tracing system to permanently label a single cell in the anterior SIA of 4 dpf *Tg(hsp70l:mCherry-T2A-CreER^{T2};fli1:LRLG;coro1a:LRLG)* reporter fish as described previously[33] and tracked the fate of the labeled SIA cells until 30 dpf, when SIA EHT near completion. Indeed, a significant number of labeled fish contained both *coro1a*:eGFP$^+$ hematopoietic cells

311 in various tissues and *fli1:*eGFP^{+} endothelial cells in the SIA (Figure 5E), strongly
312 supporting the bipotential of these SIA cells, which we term as vessel-resident
313 hemangioblasts (VRHs). Together, these findings demonstrate that the SIA comprise
314 unipotent HECs and bipotent VRHs, which generate hematopoietic cells through
315 canonical EHT and non-canonical EHT, respectively (Figure 5F).

316 **scRNA-seq analysis reveals transcriptomic signatures of cells in the supra-**
317 **intestinal artery and dorsal aorta**

318 To explore the transcriptomic characteristics of HECs and ECs in the SIA, we
319 photoconverted the anterior SIA cells in 5 dpf *Tg(kdrl:Dendra2)* zebrafish and isolated
320 the Dendra2-Red cells for scRNA-seq analysis. By combining this SIA scRNA-seq data
321 with 28 hpf DA scRNA-seq data,[40] we performed uniform manifold approximation and
322 projection (UMAP) analysis. The result revealed four distinct clusters, each cluster
323 containing cells from both DA and SIA cells, indicating a significant similarity between
324 these two hematopoietic processes (Figures 6A and 6B). Based on endothelial and
325 hematopoietic marker gene expression, we annotated the clusters as EC, HEC_1,
326 HEC_2, and HSPC (Figures 6A and 6C). The EC cluster exhibited strong expression of
327 endothelial feature genes (*etsrp*, *cdh5*, *kdrl*, *fli1*, *efnb2a*, *dll4*, *flt1*, and *hey2*), while the
328 HEC and HSPC clusters showed pronounced hematopoietic potential, as indicated by
329 the enrichment of hematopoietic markers (*gata2b*, *runx1*, *myb*, *spi2,* and *gfi1aa*,), which
330 could be further distinguished by the differing expression of terminal hematopoietic
331 genes including *coro1a*, *csf1rb*, and *ptprc* (Figure 6C). Notably, despite clear separation
332 of the four clusters, the HEC_1 and HEC_2 populations displayed a high degree of
333 similarity (Figure 6D), suggesting minimal transcriptomic differences between them.
334 Therefore, we combined the two HEC populations for subsequent comparative analysis.

335 To better understand the transcriptomic differences between the cells from the DA
336 and those from the SIA, we subdivided the EC, HEC (merged HEC_1 and HEC_2
337 populations), and HSPC populations based on origins and performed UMAP analysis
338 for each. Interestingly, while DA subpopulations were distinct and well-separated in the
339 UMAP, SIA subpopulations were intermingled (Figure 6E), indicating that

transcriptomic differences among SIA subpopulations are less pronounced compared to those between DA subpopulations. This observation aligns with the correlation analysis (Figure 6E) as well as our experimental data, which suggest that anterior SIA cells are hemogenic and lack the dorsal-ventral polarity seen in the DA (Figures 4E and 5A). Strikingly, analysis of endothelial and hematopoietic marker genes revealed that while DA_EC subpopulation strongly expressed endothelial markers but lacked hematopoietic markers, SIA_EC subpopulation not only expressed endothelial markers but also showed detectable levels of hematopoietic genes, particularly *gata2b*, a key regulator of HEC formation (Figure 6F).[61] This suggests the potential bipotency of SIA_ECs, consistent with our lineage tracing data identifying VRHs (Figures 5D-5F). Additionally, SIA_HECs and SIA_HSPCs exhibited reduced expression of key hematopoietic genes (*gata2b*, *runx1*, and *gfi1aa*) compared to their DA counterparts (Figure 6F), highlighting intrinsic differences may underlie the distinct hematopoietic processes in the SIA and DA.

To identify potential regulators essential for SIA and DA hematopoiesis, we compared their differentially expressed genes (DEGs), focusing on transcription factors (TFs). This revealed a number of candidate genes significantly enriched in either SIA or DA cells (Figure 6G). SIA-enriched TFs include *foxo4*, *hoxd3a* in SIA_ECs, *zfhx3b* and *nr4a3* in SIA_HECs, *gfi1ab* and *bcl11aa* in SIA_HSPCs (Figure 6G). Notably, *gfi1ab* and *bcl11aa* are well-documented in HSPC development and differentiation,[64-68] while the roles of the other genes remain less explored. Similarly, DA-enriched TFs included *hoxb3a*, *mafba*, and *mafbb* in the DA_ECs, *sox18*, *ldb2a*, and *her4.4* in the DA_HECs, *znf296*, *nfil3-5*, and *nfil3-6* in the DA_HSPCs (Figure 6G). Among these, *hoxb3a*, *mafba*, *mafbb*, *sox18*, *nfil3-5*, and *nfil3-6* have been implicated in hematopoiesis,[69-73] while the functions of the others are less studied. Together, these findings suggest that the distinct characteristics of SIA and DA hematopoiesis might be determined by specific sets of TFs.

DISCUSSION

In this study, using time-lapse live imaging, short-term lineage tracing with

369 photoconvertible fluorescent reporters, and permanent lineage tracing via the IR-LEGO
370 cell labeling system, we documented that zebrafish HSCs originate from the subaortic
371 SIA, rather than the DA. Furthermore, we identified bipotent VRHs in the SIA, capable
372 of generating both hematopoietic and endothelial lineages. These findings challenge the
373 conventional view of the DA as the primary source of HSCs and establish a new
374 paradigm for studying HSC development and regulatory mechanisms.

375 An intriguing unanswered question is the source of the vascular progenitors that
376 form the anterior SIA, which likely serve as precursors for HSC development. Previous
377 studies suggest that the SIA endothelium is formed by two distinct vascular progenitors:
378 ventral PCV ECs and cells derived from the extra-vascular secondary vascular field
379 (SVF).[46-48] Ventral PCV ECs sprout at approximately 28-56 hpf and migrate ventrally
380 to contribute to the SIV and SIA endothelium,[46,47] while SVF-derived cells, identified
381 as *etv2*$^{+}$*tal1*$^{+}$ vascular progenitor cells, emerge locally from the mesenchyme adjacent
382 to the ventral PCV and integrate into the SIA and SIV endothelium.[48] Given the minimal
383 contribution of ventral PCV ECs to HSC production, as shown by lineage tracing in the
384 PCV-marking *Tg(lyve1b:CreER*^{T2}*)* line (Figures 2C and 2D), we postulate that SVF-
385 derived *etv2*$^{+}$*tal1*$^{+}$ cells are the likely precursors forming the anterior SIA endothelium,
386 which then generate hematopoietic cells via EHT. Hence, developing an SVF-derived
387 cell-specific CreER^{T2} line for fate mapping analysis will be essential to validate this
388 hypothesis.

389 Another intriguing question is why the SIA generates HSCs while the DA primarily
390 produces transient hematopoietic progenitor cells — EHPs.[21] One possible explanation
391 is that the SIA and DA endothelium possess distinct intrinsic genetic/epigenetic features,
392 dictating their differing hematopoietic potential. This hypothesis is supported by the
393 scRNA-seq data, which reveals considerable transcriptomic differences between SIA
394 and DA endothelial cells (Figures 6F and 6G). These distinct characteristics may be
395 established early in development, as SIA and DA endothelium originate from different
396 vascular precursor cells.[46-48] Alternatively, extrinsic signals from the microenvironment
397 may influence the hematopoietic potential of SIA- and DA-derived cells. For instance,

398 as SIA is attached to the dorsal wall of the intestine, external cues from intestinal
399 epithelial or smooth muscle cells could shape its hematopoietic traits. Similarly, the
400 proximity of SVF cells and the SIA to pronephric duct during development[48] suggest
401 that epithelial cells of pronephros may create niches that influence HSC fate. The most
402 plausible scenario likely involves a combination of intrinsic characteristics and external
403 signals collectively regulating HSC fate in SIA-derived cells. Further investigation will
404 be essential to elucidate these mechanisms.

405 Our study reveals a striking difference in hematopoietic cell production timelines
406 between the DA and SIA. While hematopoietic cells are rapidly generated in the DA
407 within two days through canonical EHT,[6] the SIA employs both canonical and non-
408 canonical EHT processes, sustaining hematopoietic cell production for at least two
409 weeks. The coexistence of two EHT mechanisms suggests that the SIA may contain two
410 distinct precursor types: unipotent HECs, which, akin to the HECs in the DA, produce
411 hematopoietic cells through direct budding (canonical EHT), and bipotent VRHs,
412 which undergo multiple rounds of division and budding, generating both hematopoietic
413 and endothelial daughter cells (non-canonical EHT) (Figures 5D-5F; Movie S1). It
414 remains unclear whether hematopoietic cells produced through canonical EHT and non-
415 canonical EHT in the SIA differ in property and function. Given that the DA contains
416 only unipotent HECs and primarily generates EHPs through canonical EHT,[6,40] we
417 speculate that SIA-derived hematopoietic cells produced via canonical EHT are likely
418 to be EHPs, while those from non-canonical EHT are probably HSCs. The existence of
419 bipotent VRHs provokes us to hypothesize that perhaps a similar cell type may exist in
420 mammals. This hypothesis is supported by previous studies showing that the vascular
421 marker VEGFR2 enriches human postnatal HSCs and that murine bone marrow HSCs
422 can contribute to vascular endothelium upon transplantation.[74,75] The zebrafish system
423 offers a unique opportunity to explore the molecular characteristics, developmental
424 regulations, and lifespan of the VRHs, providing insights into our understanding of
425 hematopoietic and vascular system establishment and regeneration.

426 Finally, our research demonstrates that in zebrafish, HSCs primarily originate from

427 the SIA, rather than the DA, challenging the traditional view of the DA as the primary
428 source of HSCs in mammals. This discrepancy may arise from species differences, or
429 alternatively, it reflects an evolutionary conserved mechanism, suggesting an
430 alternative source for mammalian HSCs. We favor the latter possibility, in which two
431 potential models can be suggested. The first model suggests that, similar to zebrafish,
432 mammals may have an SIA-equivalent responsible for HSC production, while the DA
433 primarily generates EHPs. Given that the SIA in zebrafish is a key embryonic artery
434 dorsal to the intestine, we hypothesize that in mammals, embryonic intestinal arteries,
435 particularly those dorsal to the intestine, including the vitelline artery and its derivatives
436 like the celiac trunk and superior mesenteric artery,[76] could serve as the major sources
437 for HSC generation. This notion is supported by studies showing HSC activity in mouse
438 vitelline artery during early embryogenesis.[12,77] The second model suggests that, while
439 mammals may lack a direct SIA equivalent, HSCs could arise from a unique group of
440 subaortic mesenchyme-derived vascular precursors, similar to mesenchyme-derived
441 *etv2*$^{+}$*tal1*$^{+}$ endothelial precursors in zebrafish. In this scenario, these mesenchyme-
442 derived vascular precursors may integrate with the DA endothelium post-DA formation,
443 generating HSCs via EHT. Early studies demonstrating the presence of pre-HSCs in the
444 subaortic mesenchyme of mouse embryos during or shortly after hematopoietic cluster
445 formation in the DA support this idea.[29,30] Recent work demonstrates that tamoxifen
446 administration in *Tg(Pdgfra:CreER*^{T2}*;ROSA26:LSL-eYFP)* mice at E9.5 labels a
447 significant number of HSCs and HECs in the E11.5 DA.[78] Given that *Pdgfra* is
448 expressed in subaortic mesenchymal cells but not in the DA ECs, this finding further
449 support the notion that mammalian HSCs may originate from subaortic mesenchyme-
450 derived vascular precursors. Thus, a reevaluation of HSC origins in mammals is likely
451 warranted.

452 **METHODS**

453 **Zebrafish husbandry**

454 All fish were maintained under standard conditions.[79] The following transgenic lines
455 were used in this study: *Tg(coro1a:loxP-DsRedx-loxP-eGFP)*,[22] *Tg*(*kdrl:loxP-DsRedx-*

456 *loxP-eGFP)*^{sz100}, *Tg(hsp70l:mCherry-T2A-CreER*^{T2}*)*,[36] *Tg(lyve1b:CreER*^{T2}*)*,[80]
457 *Tg(stab1:DsRedx)*^{sz101}, *Tg(kdrl:CreER*^{T2}*)*,[81] *Tg(fli1:eGFP)*,[82] *Tg(fli1:loxP-DsRedx-*
458 *loxP-eGFP)*^{sz102}, *Tg(kdrl:eGFP)*,[83] and *Tg(kdrl:Dendra2)*[21].

459 **Generation of transgenic lines**

460 The *kdrl:loxP-DsRedx-loxP-eGFP* plasmid was created by inserting the 6.4 kb *kdrl*
461 promoter[83] and the loxP-DsRedx-loxP-eGFP cassette[22] into the pTol2 vector via Gibson
462 assembly. Similarly, the *fli1:loxP-DsRedx-loxP-eGFP* plasmid was generated with a
463 2kb *fli1* enhancer-promoter fragment.[84] A 2 kb promoter fragment upstream of the *stab1*
464 ORF was amplified (FP: CTAAGGCTTTCTAGTTGGTTGT; RP:
465 GTCTACTCCCTCAAAAGCCAG) from zebrafish genomic DNA and cloned into
466 pTol2 vectors containing the DsRedx cassette, generating the *stab1:DsRedx* plasmid.
467 To create transgenic lines, these plasmids (30 ng/μL) and in vitro transcribed
468 transposase mRNA (50 ng/μL) were co-injected into one-cell-stage AB strain embryos,
469 which were then raised to adulthood for germline transmission screening.

470 **Single-cell resolution & multi-cell resolution IR-LEGO lineage tracing**

471 The experiments were conducted according to a previous protocol with minor
472 modifications.[33] Briefly, zebrafish embryos were anesthetized using 0.02% Tricaine
473 (A5040; Sigma) and mounted in 1% low-melting agarose (A600015, Sangon Biotech).
474 For single-cell resolution lineage tracing, targeted ECs/HECs were selectively heated
475 by scanning a 1342 nm infrared light at 100 mW over a 6 mm x 8 mm area for 60
476 seconds to encompass a single cell. In multi-cell resolution lineage tracing, the infrared
477 light was applied at 110 mW over an 8 mm x 8 mm area to heat targeted cells/tissues
478 (e.g., the AGM and the SIA region). Each tissue received 3 to 4 sparse hits to label
479 multiple cells. Following infrared light illumination (heat shock), embryos were treated
480 with 10 μM (Z)-4-Hydroxytamoxifen (4-OHT) (H7904, Sigma) for 12-16 hours. After
481 washing three times with egg water, the 4-OHT-treated embryos were raised and
482 analyzed at the desired stages.

483 **Photoconversion assays**

484 To trace the behaviors and distributions of SIA-derived cells, SIA HECs/ECs in 4 dpf
485 *Tg(kdrl:Dendra2)* larvae were photoconverted using 405 nm laser with the photo-
486 bleaching program on a Zeiss 980 or Leica SP8 confocal microscope.[85] The
487 photoconverted cells were immediately imaged to record the photoconversion pattern,
488 and the distributions of their descendants were tracked for 1-4 days post-
489 photoconversion. To characterize the dynamics of SIA HEC budding, a single SIA
490 HEC/EC in the *Tg(kdrl:Dendra2)* zebrafish was photoconverted at various
491 developmental stages (3-16 dpf). The photoconverted Dendra2-Red cells were
492 subsequently tracked 24 hours post-photoconversion to determine the frequency of
493 HEC budding.

494 **Lineage tracing with tissue-specific CreER^{T2} transgenic lines**

495 To assess the contribution of PCV ECs or general vascular cells to adult HSCs, we
496 crossed the venous/lymphatic vessel-specific *Tg(lyve1b:CreERT2)* fish or pan-vessel-
497 specific *Tg(kdrl:CreER^{T2})* fish with the *Tg(kdrl:LRLG,coro1a:LRLG)* reporter line. The
498 resulting triple transgenic embryos were treated with 4-OHT (10 μM) or vehicle
499 (ethanol) from 12 hpf to 28 hpf to maximize labeling efficiency. At 3 dpf, 4-OHT-
500 treated embryos were imaged to confirm PCV labeling efficiency. Each embryo with
501 appropriate PCV or general vasculature labeling was raised to adulthood for flow
502 cytometry analysis of adult blood cell labeling efficiency.

503 **Confocal imaging and time-lapse live imaging**

504 All fluorescent images were captured with either a Zeiss 980 or Leica SP8 confocal
505 microscope with 20x and 40x air objectives or a 40x water objective. All live embryos
506 and larvae were mounted with 1% low-melting agarose in 0.5x E2 egg water. For time-
507 lapse live imaging, we used either the aforementioned confocal microscopes or
508 Olympus SpinSR spinning disc confocal microscope. Embryos and early larvae were
509 mounted in 0.7% or 1% low-melting agarose and then covered with 0.02% Tricaine in
510 0.5x E2 egg water after the agarose solidified. Imaging dishes included 35 mm glass
511 bottom confocal dishes (biosharp, BS-15-GJM) or μ-Slide 8 Well (ibidi, 80826),
512 depending on the number of samples. Dishes were placed in a heating device to

513 maintain a stable temperature of 28.5 °C. Each imaging cycle was set for 15-20 minutes,
514 and the samples were sequentially imaged over 12-48 hours to capture long-term cell
515 behaviors. Images were processed with FIJI (ImageJ), except for Z-stack color-coding,
516 which was processed via Zeiss ZEN 3.7 software.

517 **Single-cell suspension preparation and flow cytometry analysis**

518 To assess the labeling efficiency of adult zebrafish KM blood cells, KM from
519 euthanized adult zebrafish (3-12 months) were collected and mechanically dissociated
520 in 400uL ice-cold 5% FBS/PBS buffer. The suspension was filtered through a 35 μm
521 cell strainer (352235, Corning Falcon) to obtain a single-cell suspension for analysis.
522 Flow cytometry analysis was performed using a BD FACSAria III flow cytometer, and
523 data analysis, including gating image generation, was conducted using FlowJo
524 (v10.8.1).

525 **Notch inhibitor treatment**

526 The γ-secretase inhibitor DAPT powder (D5942, Sigma-Aldrich) was dissolved in
527 DMSO to prepare a 100 mM stock solution. For experiments, 10 μL of the stock
528 solution was mixed with 10 mL of 0.5x E2 embryo media to treat larvae aged 2.5-3.5
529 dpf, 3.5-4.5 dpf, and 2.5-4.5 dpf. In the control group, 10 μL of DMSO was mixed with
530 the same volume of 0.5x E2 embryo media. After treatment, larvae were transferred to
531 regular 0.5x E2 embryo media or system water for further development until subsequent
532 assays.

533 **Manual cell picking and Smart-seq2 scRNA-seq sample processing**

534 To prepare single-cell suspension for manual cell picking, 5 dpf *Tg(kdrl:Dendra2)*
535 larvae with photoconverted anterior SIA were anesthetized using 0.02% Tricaine
536 (E10521, Sigma-Aldrich). Trunk containing photoconverted SIA was dissected from
537 ~80-100 larvae, washed with ice-cold 5% FBS/PBS buffer, and mechanically
538 disassociated using 26 G needles and syringes. The dissociated tissues were
539 enzymatically digested with EDTA-free TrypLE™ Express enzyme (12605028, Gibco)
540 for 10 min, followed by 1:1 mixed TrypLE™ Express and StemPro™ Accutase™

541 (A1110501, Gibco) for an additional 10 min. The digestion reaction was stopped by
542 adding FBS to a final concentration of 10%. Digested cells were harvested by standard
543 centrifugation, washed, and resuspended in ice-cold 1% BSA/DPBS (14190144, Gibco)
544 buffer. Finally, the cell suspension was filtered through a 35 μm cell strainer to obtain
545 a single-cell suspension.

546 To pick photoconverted cells, 20 μL of the single-cell suspension was carefully
547 loaded into an uncoated sterile culture dish. Individual photoconverted cells were
548 collected using an IM-9C pneumatic injector (Narishige) under a fluorescent
549 microscope and immediately transferred into sterile 200 μL PCR tubes preloaded with
550 4.4 μL lysis buffer. Immediately following the transfer, the cells were vortexed, spun
551 down, and stored at -80°C.

552 Whole-transcriptome amplification and library preparation were performed
553 following the Smart-seq2 protocol.[86,87] Library quality was evaluated using either the
554 Agilent 5300 Fragment Analyzer or the BiOptic Qsep100 Fragment Analyzer. Prepared
555 libraries were sent to Novogene for Illumina 150-bp paired-end sequencing, with an
556 average sequencing depth of 2 Gb per sample.

557 **scRNA-seq data integration and analysis.**

558 For scRNA-seq data analysis, reads were aligned to the GRCz11.113 zebrafish
559 reference genome using the STAR package (2.5.2b),[88] and gene counts were quantified
560 with featureCounts (Rsubread_2.20.0). The resulting count matrices were normalized
561 to transcripts per million (TPM) for downstream analysis. Datasets from 5 dpf SIA and
562 28 hpf-DA photoconverted cells were processed and analyzed using the Seurat package
563 (v.5.1.0).

564 Prior to analysis, quality control was performed using the following criteria:
565 nCount_RNA > 200, nFeature_RNA < 2000, and percent.mt < 5. After filtering, 181
566 cells were retained for analysis. Principal component analysis (PCA) was performed,
567 followed by data scaling. To minimize batch effect, the Harmony algorithm was applied
568 as part of the standard integration workflow
569 (https://satijalab.org/seurat/articles/seurat5_integration). Clustering analysis was

conducted, and visualization was accomplished through dimensionality reduction using UMAP based on shared nearest-neighbor clustering. Dot plots, feature plots, and violin plots were generated to visualize gene expression patterns using SCT-normalized data. GO enrichment analysis was performed with the clusterProfiler package (v.4.14.4), using marker genes filtered by a minimum percentage of cells expressing the gene (min.pct = 0.25) and a log fold change threshold (logfc.threshold = 0.25). All analyses were conducted within the R environment (v.4.4.2).

Quantifications and statistics

Statistical parameters, including the exact value of n, are reported in the figures and figure legends. Data are presented as means ± SD whenever applicable. Statistical significance is denoted as follows: ns, $P>0.05$; * $P \leq 0.05$; ** $P \leq 0.01$; *** $P \leq 0.001$, and **** $P \leq 0.0001$. Depending on variance homogeneity, unpaired Student's t-test or Welch's t-test were used to calculate P values. All statistical analyses were performed using GraphPad Prism version 10.

ACKNOWLEDGEMENTS

This work was supported by grants from the National Key Research and Development Program of China (2023YFA1800100), the Shenzhen Medical Research Fund (B2302034), and the Research Grants Council of Hong Kong (T13-602/21-N).

AUTHOR CONTRIBUTIONS

Z.W. and S.F. conceived the project, designed the experiments, and wrote the manuscript. S.F. and R.Q. performed all the experiments. S.H., Y.H., and T.H. provided the single-cell resolution IR-LEGO system and assisted with lineage tracing experiments. Y.W., T.T., K.C., S.Z., Y.H., and H.Z provided additional experimental support.

DECLARATION OF INTERESTS

The authors declare no competing interests.

REFERENCES

1. Kondo, M., Wagers, A.J., Manz, M.G., Prohaska, S.S., Scherer, D.C., Beilhack, G.F., Shizuru, J.A., and Weissman, I.L. (2003). Biology of hematopoietic stem cells and progenitors: implications for clinical application. Annu Rev Immunol *21*, 759-806. 10.1146/annurev.immunol.21.120601.141007.
2. Pinho, S., and Frenette, P.S. (2019). Haematopoietic stem cell activity and interactions with the niche. Nat Rev Mol Cell Biol *20*, 303-320. 10.1038/s41580-019-0103-9.
3. Passegue, E., Jamieson, C.H., Ailles, L.E., and Weissman, I.L. (2003). Normal and leukemic hematopoiesis: are leukemias a stem cell disorder or a reacquisition of stem cell characteristics? Proceedings of the National Academy of Sciences of the United States of America *100 Suppl 1*, 11842-11849. 10.1073/pnas.2034201100.
4. Chabannon, C., Kuball, J., Bondanza, A., Dazzi, F., Pedrazzoli, P., Toubert, A., Ruggeri, A., Fleischhauer, K., and Bonini, C. (2018). Hematopoietic stem cell transplantation in its 60s: A platform for cellular therapies. Sci Transl Med *10*. 10.1126/scitranslmed.aap9630.
5. Hutter, G., and Zaia, J.A. (2011). Allogeneic haematopoietic stem cell transplantation in patients with human immunodeficiency virus: the experiences of more than 25 years. Clin Exp Immunol *163*, 284-295. 10.1111/j.1365-2249.2010.04312.x.
6. Kissa, K., and Herbomel, P. (2010). Blood stem cells emerge from aortic endothelium by a novel type of cell transition. Nature *464*, 112-115. 10.1038/nature08761.
7. Bertrand, J.Y., Chi, N.C., Santoso, B., Teng, S., Stainier, D.Y., and Traver, D. (2010). Haematopoietic stem cells derive directly from aortic endothelium during development. Nature *464*, 108-111. 10.1038/nature08738.
8. Boisset, J.C., van Cappellen, W., Andrieu-Soler, C., Galjart, N., Dzierzak, E., and Robin, C. (2010). In vivo imaging of haematopoietic cells emerging from the mouse aortic endothelium. Nature *464*, 116-120. 10.1038/nature08764.
9. Jaffredo, T., Gautier, R., Eichmann, A., and Dieterlen-Lievre, F. (1998). Intraaortic hemopoietic cells are derived from endothelial cells during ontogeny. Development *125*, 4575-4583. 10.1242/dev.125.22.4575.
10. Muller, A.M., Medvinsky, A., Strouboulis, J., Grosveld, F., and Dzierzak, E. (1994). Development of hematopoietic stem cell activity in the mouse embryo. Immunity *1*, 291-301.
11. Medvinsky, A., and Dzierzak, E. (1996). Definitive hematopoiesis is autonomously initiated by the AGM region. Cell *86*, 897-906. 10.1016/s0092-8674(00)80165-8.
12. de Bruijn, M.F.T.R., Speck, N.A., Peeters, M.C.E., and Dzierzak, E. (2000). Definitive hematopoietic stem cells first develop within the major arterial regions of the mouse embryo. Embo Journal *19*, 2465-2474. DOI 10.1093/emboj/19.11.2465.
13. de Jong, J.L.O., and Zon, L.I. (2005). Use of the zebrafish system to study primitive and definitive hematopoiesis. Annu Rev Genet *39*, 481-501. 10.1146/annurev.genet.39.073003.095931.
14. Lam, E.Y., Chau, J.Y., Kalev-Zylinska, M.L., Fountaine, T.M., Mead, R.S., Hall, C.J., Crosier, P.S., Crosier, K.E., and Flores, M.V. (2009). Zebrafish runx1 promoter-EGFP transgenics mark discrete sites of definitive blood progenitors. Blood *113*, 1241-1249. 10.1182/blood-2008-04-149898.
15. Zhen, F., Lan, Y., Yan, B., Zhang, W., and Wen, Z. (2013). Hemogenic endothelium specification and hematopoietic stem cell maintenance employ distinct Scl isoforms. Development *140*, 3977-3985. 10.1242/dev.097071.

641 16. Bonkhofer, F., Rispoli, R., Pinheiro, P., Krecsmarik, M., Schneider-Swales, J., Tsang, I.H.C., de
642 Bruijn, M., Monteiro, R., Peterkin, T., and Patient, R. (2019). Blood stem cell-forming
643 haemogenic endothelium in zebrafish derives from arterial endothelium. Nature
644 communications *10*, 3577. 10.1038/s41467-019-11423-2.
645 17. Zovein, A.C., Hofmann, J.J., Lynch, M., French, W.J., Turlo, K.A., Yang, Y., Becker, M.S.,
646 Zanetta, L., Dejana, E., Gasson, J.C., et al. (2008). Fate tracing reveals the endothelial origin of
647 hematopoietic stem cells. Cell stem cell *3*, 625-636. 10.1016/j.stem.2008.09.018.
648 18. de Bruijn, M.F., Ma, X., Robin, C., Ottersbach, K., Sanchez, M.J., and Dzierzak, E. (2002).
649 Hematopoietic stem cells localize to the endothelial cell layer in the midgestation mouse aorta.
650 Immunity *16*, 673-683. 10.1016/s1074-7613(02)00313-8.
651 19. Garcia-Porrero, J.A., Godin, I.E., and Dieterlen-Lievre, F. (1995). Potential intraembryonic
652 hemogenic sites at pre-liver stages in the mouse. Anat Embryol (Berl) *192*, 425-435.
653 10.1007/BF00240375.
654 20. Yokomizo, T., and Dzierzak, E. (2010). Three-dimensional cartography of hematopoietic
655 clusters in the vasculature of whole mouse embryos. Development *137*, 3651-3661.
656 10.1242/dev.051094.
657 21. Tian, Y., Xu, J., Feng, S., He, S., Zhao, S., Zhu, L., Jin, W., Dai, Y., Luo, L., Qu, J.Y., and Wen,
658 Z. (2017). The first wave of T lymphopoiesis in zebrafish arises from aorta endothelium
659 independent of hematopoietic stem cells. J Exp Med. 10.1084/jem.20170488.
660 22. Xu, J., Zhu, L., He, S., Wu, Y., Jin, W., Yu, T., Qu, J.Y., and Wen, Z. (2015). Temporal-Spatial
661 Resolution Fate Mapping Reveals Distinct Origins for Embryonic and Adult Microglia in
662 Zebrafish. Developmental cell *34*, 632-641. 10.1016/j.devcel.2015.08.018.
663 23. He, S., Chen, J., Jiang, Y., Wu, Y., Zhu, L., Jin, W., Zhao, C., Yu, T., Wang, T., Wu, S., et al.
664 (2018). Adult zebrafish Langerhans cells arise from hematopoietic stem/progenitor cells. Elife
665 *7*. 10.7554/eLife.36131.
666 24. Taoudi, S., Gonneau, C., Moore, K., Sheridan, J.M., Blackburn, C.C., Taylor, E., and Medvinsky,
667 A. (2008). Extensive hematopoietic stem cell generation in the AGM region via maturation of
668 VE-cadherin+CD45+ pre-definitive HSCs. Cell stem cell *3*, 99-108.
669 10.1016/j.stem.2008.06.004.
670 25. Medvinsky, A., Rybtsov, S., and Taoudi, S. (2011). Embryonic origin of the adult hematopoietic
671 system: advances and questions. Development *138*, 1017-1031. 10.1242/dev.040998.
672 26. Taoudi, S., and Medvinsky, A. (2007). Functional identification of the hematopoietic stem cell
673 niche in the ventral domain of the embryonic dorsal aorta. Proceedings of the National Academy
674 of Sciences of the United States of America *104*, 9399-9403. 10.1073/pnas.0700984104.
675 27. North, T.E., de Bruijn, M.F., Stacy, T., Talebian, L., Lind, E., Robin, C., Binder, M., Dzierzak,
676 E., and Speck, N.A. (2002). Runx1 expression marks long-term repopulating hematopoietic
677 stem cells in the midgestation mouse embryo. Immunity *16*, 661-672.
678 28. Beaudin, A.E., Boyer, S.W., Perez-Cunningham, J., Hernandez, G.E., Derderian, S.C.,
679 Jujjavarapu, C., Aaserude, E., MacKenzie, T., and Forsberg, E.C. (2016). A Transient
680 Developmental Hematopoietic Stem Cell Gives Rise to Innate-like B and T Cells. Cell stem cell.
681 10.1016/j.stem.2016.08.013.
682 29. Rybtsov, S., Sobiesiak, M., Taoudi, S., Souilhol, C., Senserrich, J., Liakhovitskaia, A., Ivanovs,
683 A., Frampton, J., Zhao, S., and Medvinsky, A. (2011). Hierarchical organization and early
684 hematopoietic specification of the developing HSC lineage in the AGM region. The Journal of

experimental medicine *208*, 1305-1315. 10.1084/jem.20102419.

30. Bertrand, J.Y., Giroux, S., Golub, R., Klaine, M., Jalil, A., Boucontet, L., Godin, I., and Cumano, A. (2005). Characterization of purified intraembryonic hematopoietic stem cells as a tool to define their site of origin. Proceedings of the National Academy of Sciences of the United States of America *102*, 134-139. 10.1073/pnas.0402270102.

31. Dignum, T., Varnum-Finney, B., Srivatsan, S.R., Dozono, S., Waltner, O., Heck, A.M., Ishida, T., Nourigat-McKay, C., Jackson, D.L., Rafii, S., et al. (2021). Multipotent progenitors and hematopoietic stem cells arise independently from hemogenic endothelium in the mouse embryo. Cell reports *36*, 109675. 10.1016/j.celrep.2021.109675.

32. Patel, S.H., Christodoulou, C., Weinreb, C., Yu, Q., da Rocha, E.L., Pepe-Mooney, B.J., Bowling, S., Li, L., Osorio, F.G., Daley, G.Q., and Camargo, F.D. (2022). Lifelong multilineage contribution by embryonic-born blood progenitors. Nature *606*, 747-753. 10.1038/s41586-022-04804-z.

33. He, S., Tian, Y., Feng, S., Wu, Y., Shen, X., Chen, K., He, Y., Sun, Q., Li, X., Xu, J., et al. (2020). In vivo single-cell lineage tracing in zebrafish using high-resolution infrared laser-mediated gene induction microscopy. Elife *9*. 10.7554/eLife.52024.

34. Kobayashi, M., Wei, H., Yamanashi, T., Azevedo Portilho, N., Cornelius, S., Valiente, N., Nishida, C., Cheng, H., Latorre, A., Zheng, W.J., et al. (2023). HSC-independent definitive hematopoiesis persists into adult life. Cell reports *42*, 112239. 10.1016/j.celrep.2023.112239.

35. Dzierzak, E., and Bigas, A. (2018). Blood Development: Hematopoietic Stem Cell Dependence and Independence. Cell stem cell *22*, 639-651. 10.1016/j.stem.2018.04.015.

36. Hans, S., Freudenreich, D., Geffarth, M., Kaslin, J., Machate, A., and Brand, M. (2011). Generation of a non-leaky heat shock-inducible Cre line for conditional Cre/lox strategies in zebrafish. Dev Dyn *240*, 108-115. 10.1002/dvdy.22497.

37. Li, L., Yan, B., Shi, Y.Q., Zhang, W.Q., and Wen, Z.L. (2012). Live imaging reveals differing roles of macrophages and neutrophils during zebrafish tail fin regeneration. The Journal of biological chemistry *287*, 25353-25360. 10.1074/jbc.M112.349126.

38. Traver, D., Paw, B.H., Poss, K.D., Penberthy, W.T., Lin, S., and Zon, L.I. (2003). Transplantation and in vivo imaging of multilineage engraftment in zebrafish bloodless mutants. Nature immunology *4*, 1238-1246. 10.1038/ni1007.

39. Henninger, J., Santoso, B., Hans, S., Durand, E., Moore, J., Mosimann, C., Brand, M., Traver, D., and Zon, L. (2017). Clonal fate mapping quantifies the number of haematopoietic stem cells that arise during development. Nat Cell Biol *19*, 17-27. 10.1038/ncb3444.

40. Zhao, S., Feng, S., Tian, Y., and Wen, Z. (2022). Hemogenic and aortic endothelium arise from a common hemogenic angioblast precursor and are specified by the Etv2 dosage. Proceedings of the National Academy of Sciences of the United States of America *119*, e2119051119. 10.1073/pnas.2119051119.

41. Gerlach, G.F., and Wingert, R.A. (2013). Kidney organogenesis in the zebrafish: insights into vertebrate nephrogenesis and regeneration. Wiley Interdiscip Rev Dev Biol *2*, 559-585. 10.1002/wdev.92.

42. Diep, C.Q., Ma, D., Deo, R.C., Holm, T.M., Naylor, R.W., Arora, N., Wingert, R.A., Bollig, F., Djordjevic, G., Lichman, B., et al. (2011). Identification of adult nephron progenitors capable of kidney regeneration in zebrafish. Nature *470*, 95-100. 10.1038/nature09669.

43. Ye, D., Zhu, L., Zhang, Q., Xiong, F., Wang, H., Wang, X., He, M., Zhu, Z., and Sun, Y. (2019).

Abundance of Early Embryonic Primordial Germ Cells Promotes Zebrafish Female Differentiation as Revealed by Lifetime Labeling of Germline. Mar Biotechnol (NY) *21*, 217-228. 10.1007/s10126-019-09874-1.

44. Isogai, S., Horiguchi, M., and Weinstein, B.M. (2001). The vascular anatomy of the developing zebrafish: an atlas of embryonic and early larval development. Developmental biology *230*, 278-301. 10.1006/dbio.2000.9995.

45. Chen, J., Li, X., Ni, R., Chen, Q., Yang, Q., He, J., and Luo, L. (2021). Acute brain vascular regeneration occurs via lymphatic transdifferentiation. Developmental cell *56*, 3115-3127 e3116. 10.1016/j.devcel.2021.09.005.

46. Hen, G., Nicenboim, J., Mayseless, O., Asaf, L., Shin, M., Busolin, G., Hofi, R., Almog, G., Tiso, N., Lawson, N.D., and Yaniv, K. (2015). Venous-derived angioblasts generate organ-specific vessels during zebrafish embryonic development. Development *142*, 4266-4278. 10.1242/dev.129247.

47. Koenig, A.L., Baltrunaite, K., Bower, N.I., Rossi, A., Stainier, D.Y., Hogan, B.M., and Sumanas, S. (2016). Vegfa signaling promotes zebrafish intestinal vasculature development through endothelial cell migration from the posterior cardinal vein. Developmental biology *411*, 115-127. 10.1016/j.ydbio.2016.01.002.

48. Metikala, S., Warkala, M., Casie Chetty, S., Chestnut, B., Rufin Florat, D., Plender, E., Nester, O., Koenig, A.L., Astrof, S., and Sumanas, S. (2022). Integration of vascular progenitors into functional blood vessels represents a distinct mechanism of vascular growth. Developmental cell. 10.1016/j.devcel.2022.02.015.

49. Goi, M., and Childs, S.J. (2016). Patterning mechanisms of the sub-intestinal venous plexus in zebrafish. Developmental biology *409*, 114-128. 10.1016/j.ydbio.2015.10.017.

50. Murayama, E., Kissa, K., Zapata, A., Mordelet, E., Briolat, V., Lin, H.F., Handin, R.I., and Herbomel, P. (2006). Tracing hematopoietic precursor migration to successive hematopoietic organs during zebrafish development. Immunity *25*, 963-975. 10.1016/j.immuni.2006.10.015.

51. Jin, H., Xu, J., and Wen, Z. (2007). Migratory path of definitive hematopoietic stem/progenitor cells during zebrafish development. Blood *109*, 5208-5214. 10.1182/blood-2007-01-069005.

52. Kimmel, C.B., Ballard, W.W., Kimmel, S.R., Ullmann, B., and Schilling, T.F. (1995). Stages of embryonic development of the zebrafish. Dev Dyn *203*, 253-310. 10.1002/aja.1002030302.

53. Chen, M.J., Yokomizo, T., Zeigler, B.M., Dzierzak, E., and Speck, N.A. (2009). Runx1 is required for the endothelial to haematopoietic cell transition but not thereafter. Nature *457*, 887-891. 10.1038/nature07619.

54. Jin, H., Sood, R., Xu, J., Zhen, F., English, M.A., Liu, P.P., and Wen, Z. (2009). Definitive hematopoietic stem/progenitor cells manifest distinct differentiation output in the zebrafish VDA and PBI. Development *136*, 647-654. 10.1242/dev.029637.

55. Sood, R., English, M.A., Belele, C.L., Jin, H., Bishop, K., Haskins, R., McKinney, M.C., Chahal, J., Weinstein, B.M., Wen, Z., and Liu, P.P. (2010). Development of multilineage adult hematopoiesis in the zebrafish with a runx1 truncation mutation. Blood *115*, 2806-2809. 10.1182/blood-2009-08-236729.

56. Kumano, K., Chiba, S., Kunisato, A., Sata, M., Saito, T., Nakagami-Yamaguchi, E., Yamaguchi, T., Masuda, S., Shimizu, K., Takahashi, T., et al. (2003). Notch1 but not Notch2 is essential for generating hematopoietic stem cells from endothelial cells. Immunity *18*, 699-711. 10.1016/s1074-7613(03)00117-1.

57. Burns, C.E., Traver, D., Mayhall, E., Shepard, J.L., and Zon, L.I. (2005). Hematopoietic stem cell fate is established by the Notch-Runx pathway. Gene Dev *19*, 2331-2342. 10.1101/gad.1337005.
58. Hadland, B.K., Huppert, S.S., Kanungo, J., Xue, Y., Jiang, R., Gridley, T., Conlon, R.A., Cheng, A.M., Kopan, R., and Longmore, G.D. (2004). A requirement for Notch1 distinguishes 2 phases of definitive hematopoiesis during development. Blood *104*, 3097-3105. 10.1182/blood-2004-03-1224.
59. Clements, W.K., Kim, A.D., Ong, K.G., Moore, J.C., Lawson, N.D., and Traver, D. (2011). A somitic Wnt16/Notch pathway specifies haematopoietic stem cells. Nature *474*, 220-224. 10.1038/nature10107.
60. Geling, A., Steiner, H., Willem, M., Bally-Cuif, L., and Haass, C. (2002). A gamma-secretase inhibitor blocks Notch signaling in vivo and causes a severe neurogenic phenotype in zebrafish. EMBO Rep *3*, 688-694. 10.1093/embo-reports/kvf124.
61. Butko, E., Distel, M., Pouget, C., Weijts, B., Kobayashi, I., Ng, K., Mosimann, C., Poulain, F.E., McPherson, A., Ni, C.W., et al. (2015). Gata2b is a restricted early regulator of hemogenic endothelium in the zebrafish embryo. Development *142*, 1050-1061. 10.1242/dev.119180.
62. Robert-Moreno, A., Guiu, J., Ruiz-Herguido, C., Lopez, M.E., Ingles-Esteve, J., Riera, L., Tipping, A., Enver, T., Dzierzak, E., Gridley, T., et al. (2008). Impaired embryonic haematopoiesis yet normal arterial development in the absence of the Notch ligand Jagged1. The EMBO journal *27*, 1886-1895. 10.1038/emboj.2008.113.
63. Gurskaya, N.G., Verkhusha, V.V., Shcheglov, A.S., Staroverov, D.B., Chepurnykh, T.V., Fradkov, A.F., Lukyanov, S., and Lukyanov, K.A. (2006). Engineering of a monomeric green-to-red photoactivatable fluorescent protein induced by blue light. Nat Biotechnol *24*, 461-465. 10.1038/nbt1191.
64. Yu, Y., Wang, J., Khaled, W., Burke, S., Li, P., Chen, X., Yang, W., Jenkins, N.A., Copeland, N.G., Zhang, S., and Liu, P. (2012). Bcl11a is essential for lymphoid development and negatively regulates p53. The Journal of experimental medicine *209*, 2467-2483. 10.1084/jem.20121846.
65. Tsang, J.C., Yu, Y., Burke, S., Buettner, F., Wang, C., Kolodziejczyk, A.A., Teichmann, S.A., Lu, L., and Liu, P. (2015). Single-cell transcriptomic reconstruction reveals cell cycle and multi-lineage differentiation defects in Bcl11a-deficient hematopoietic stem cells. Genome Biol *16*, 178. 10.1186/s13059-015-0739-5.
66. Luc, S., Huang, J., McEldoon, J.L., Somuncular, E., Li, D., Rhodes, C., Mamoor, S., Hou, S., Xu, J., and Orkin, S.H. (2016). Bcl11a Deficiency Leads to Hematopoietic Stem Cell Defects with an Aging-like Phenotype. Cell reports *16*, 3181-3194. 10.1016/j.celrep.2016.08.064.
67. Thambyrajah, R., Ucanok, D., Jalali, M., Hough, Y., Wilkinson, R.N., McMahon, K., Moore, C., and Gering, M. (2016). A gene trap transposon eliminates haematopoietic expression of zebrafish Gfi1aa, but does not interfere with haematopoiesis. Developmental biology *417*, 25-39. 10.1016/j.ydbio.2016.07.010.
68. Hock, H., Hamblen, M.J., Rooke, H.M., Schindler, J.W., Saleque, S., Fujiwara, Y., and Orkin, S.H. (2004). Gfi-1 restricts proliferation and preserves functional integrity of haematopoietic stem cells. Nature *431*, 1002-1007. 10.1038/nature02994.
69. Jung, H.S., Suknuntha, K., Kim, Y.H., Liu, P., Dettle, S.T., Sedzro, D.M., Smith, P.R., Thomson, J.A., Ong, I.M., and Slukvin, II (2023). SOX18-enforced expression diverts hemogenic

endothelium-derived progenitors from T towards NK lymphoid pathways. iScience *26*, 106621. 10.1016/j.isci.2023.106621.

70. Sauvageau, G., Thorsteinsdottir, U., Hough, M.R., Hugo, P., Lawrence, H.J., Largman, C., and Humphries, R.K. (1997). Overexpression of HOXB3 in hematopoietic cells causes defective lymphoid development and progressive myeloproliferation. Immunity *6*, 13-22. 10.1016/s1074-7613(00)80238-1.

71. Ko, K.H., Lam, Q.L., Zhang, M., Wong, C.K., Lo, C.K., Kahmeyer-Gabbe, M., Tsang, W.H., Tsang, S.L., Chan, L.C., Sham, M.H., and Lu, L. (2007). Hoxb3 deficiency impairs B lymphopoiesis in mouse bone marrow. Exp Hematol *35*, 465-475. 10.1016/j.exphem.2006.10.014.

72. Kelly, L.M., Englmeier, U., Lafon, I., Sieweke, M.H., and Graf, T. (2000). MafB is an inducer of monocytic differentiation. EMBO J *19*, 1987-1997. 10.1093/emboj/19.9.1987.

73. Yu, X., Wang, Y., Deng, M., Li, Y., Ruhn, K.A., Zhang, C.C., and Hooper, L.V. (2014). The basic leucine zipper transcription factor NFIL3 directs the development of a common innate lymphoid cell precursor. Elife *3*. 10.7554/eLife.04406.

74. Ziegler, B.L., Valtieri, M., Porada, G.A., De Maria, R., Muller, R., Masella, B., Gabbianelli, M., Casella, I., Pelosi, E., Bock, T., et al. (1999). KDR receptor: a key marker defining hematopoietic stem cells. Science *285*, 1553-1558. 10.1126/science.285.5433.1553.

75. Bailey, A.S., Jiang, S., Afentoulis, M., Baumann, C.I., Schroeder, D.A., Olson, S.B., Wong, M.H., and Fleming, W.H. (2004). Transplanted adult hematopoietic stems cells differentiate into functional endothelial cells. Blood *103*, 13-19. 10.1182/blood-2003-05-1684.

76. Lung, K., and Lui, F. (2025). Anatomy, Abdomen and Pelvis: Arteries. In StatPearls.

77. Gordon-Keylock, S., Sobiesiak, M., Rybtsov, S., Moore, K., and Medvinsky, A. (2013). Mouse extraembryonic arterial vessels harbor precursors capable of maturing into definitive HSCs. Blood *122*, 2338-2345. 10.1182/blood-2012-12-470971.

78. Chandrakanthan, V., Rorimpandey, P., Zanini, F., Chacon, D., Olivier, J., Joshi, S., Kang, Y.C., Knezevic, K., Huang, Y., Qiao, Q., et al. (2022). Mesoderm-derived PDGFRA(+) cells regulate the emergence of hematopoietic stem cells in the dorsal aorta. Nat Cell Biol *24*, 1211-1225. 10.1038/s41556-022-00955-3.

79. Westerfield, M., and ZFIN. (2000). The zebrafish book : a guide for the laboratory use of zebrafish Danio (Brachydanio) rerio, 4th Edition (ZFIN).

80. Chen, J., He, J., Ni, R., Yang, Q., Zhang, Y., and Luo, L. (2019). Cerebrovascular Injuries Induce Lymphatic Invasion into Brain Parenchyma to Guide Vascular Regeneration in Zebrafish. Dev Cell *49*, 697-710 e695. 10.1016/j.devcel.2019.03.022.

81. Zhao, L., Borikova, A.L., Ben-Yair, R., Guner-Ataman, B., MacRae, C.A., Lee, R.T., Burns, C.G., and Burns, C.E. (2014). Notch signaling regulates cardiomyocyte proliferation during zebrafish heart regeneration. Proc Natl Acad Sci U S A *111*, 1403-1408. 10.1073/pnas.1311705111.

82. Roman, B.L., Pham, V.N., Lawson, N.D., Kulik, M., Childs, S., Lekven, A.C., Garrity, D.M., Moon, R.T., Fishman, M.C., Lechleider, R.J., and Weinstein, B.M. (2002). Disruption of acvrl1 increases endothelial cell number in zebrafish cranial vessels. Development *129*, 3009-3019. 10.1242/dev.129.12.3009.

83. Jin, S.W., Beis, D., Mitchell, T., Chen, J.N., and Stainier, D.Y. (2005). Cellular and molecular analyses of vascular tube and lumen formation in zebrafish. Development *132*, 5199-5209.

861 10.1242/dev.02087.
862 84. Villefranc, J.A., Amigo, J., and Lawson, N.D. (2007). Gateway compatible vectors for analysis
863 of gene function in the zebrafish. Dev Dyn *236*, 3077-3087. 10.1002/dvdy.21354.
864 85. Dixon, G., Elks, P.M., Loynes, C.A., Whyte, M.K., and Renshaw, S.A. (2012). A method for the
865 in vivo measurement of zebrafish tissue neutrophil lifespan. ISRN Hematol *2012*, 915868.
866 10.5402/2012/915868.
867 86. Picelli, S., Faridani, O.R., Bjorklund, A.K., Winberg, G., Sagasser, S., and Sandberg, R. (2014).
868 Full-length RNA-seq from single cells using Smart-seq2. Nat Protoc *9*, 171-181.
869 10.1038/nprot.2014.006.
870 87. Wu, S., Nguyen, L.T.M., Pan, H., Hassan, S., Dai, Y., Xu, J., and Wen, Z. (2020). Two
871 phenotypically and functionally distinct microglial populations in adult zebrafish. Sci Adv *6*.
872 10.1126/sciadv.abd1160.
873 88. Dobin, A., Davis, C.A., Schlesinger, F., Drenkow, J., Zaleski, C., Jha, S., Batut, P., Chaisson,
874 M., and Gingeras, T.R. (2013). STAR: ultrafast universal RNA-seq aligner. Bioinformatics *29*,
875 15-21. 10.1093/bioinformatics/bts635.
876

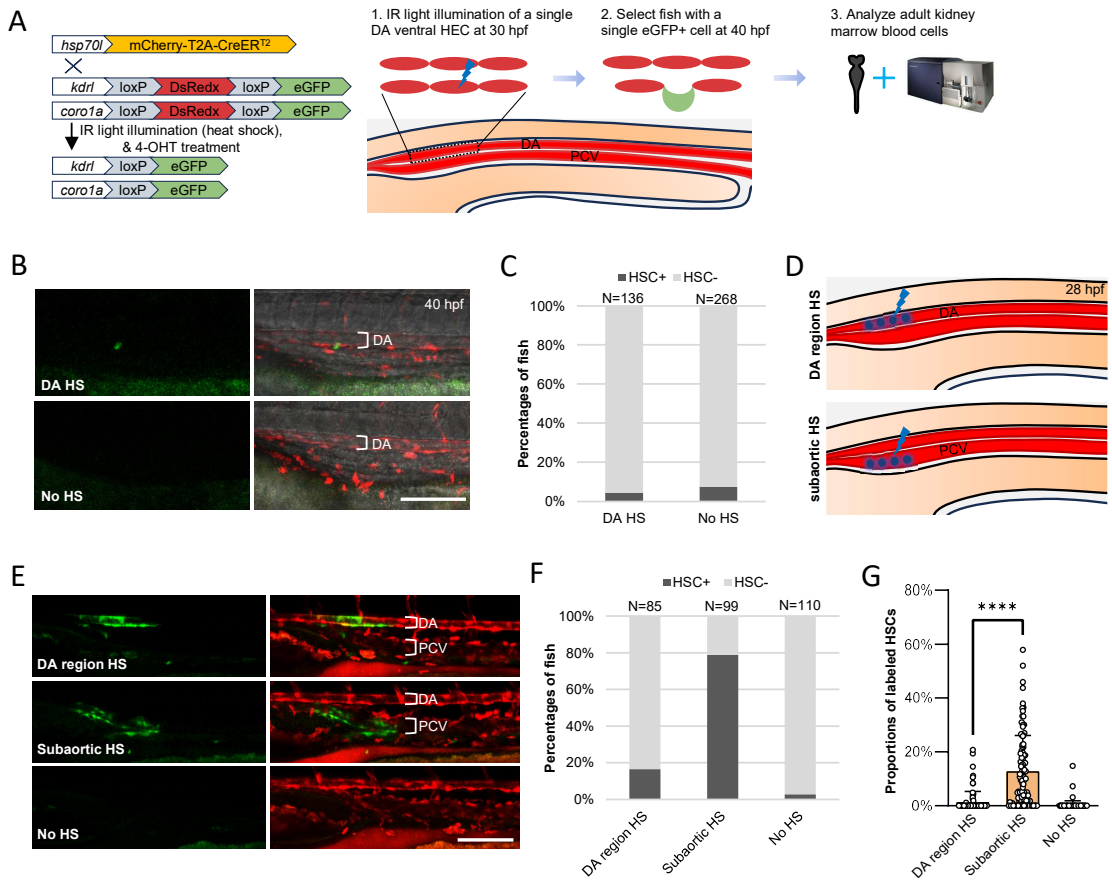

Figure 1. HSCs in zebrafish do not originate from the DA

(A) The left panel illustrates the principle of the single-cell resolution IR-LEGO lineage tracing strategy. In 30 hpf *Tg(hsp70l:mCherry-T2A-CreER^{T2};kdrl:LRLG;coro1a:LRLG)* embryos, a single HEC is illuminated by infrared light (heat shock) followed by 4-OHT treatment, inducing CreER^{T2}-mediated recombination of the reporter genes. This results in the targeted single HEC and its hematopoietic progeny switching from DsRedx to eGFP expression. The right panel outlines the experimental pipeline. DA: dorsal aorta. PCV: posterior cardinal vein.

(B) Representative images of a successful single cell-labeled fish (upper panel) and a control fish (lower panel). 10 hours post-IR illumination, fish with single HEC labeling (eGFP^{+}) in the DA, confirmed by confocal microscopy, were selected for further analysis. Scale bar: 100 μm (all scale bars hereafter are 100 μm unless otherwise annotated). HS: heat shock.

(C) Summary of the ratios of HSC-labeled fish in the single cell-labeled (DA HS) and control (No HS) groups, based on flow cytometry analysis of adult kidney marrow blood cells (3 to 12 months fish) (Fig. S1A and S1B). 136 DA HS fish (N=136) and 268 control fish (N=268) were evaluated. The data is a combination of 22 independent experiments. In each experiment, 4-8 single cell-labeled fish were obtained from 20-30 infrared light-illuminated fish.

(D) Schematic illustration of multi-cell resolution infrared light-mediated labeling of one somite-width DA region or subaortic AGM region between 8th and 10th somite.

(E) Representative images of DA-labeled, subaortic AGM region-labeled, and control (No HS) fish. Fish with relatively region-specific $eGFP^{+}$ vasculature pattern observed via confocal microscopy on 3 dpf were selected and survived to adulthood for further analysis.

(F) The ratios of HSC-labeled fish in the three groups. The results are derived from a combination of 11 independent experiments to ensure sufficient sample size for reliable percentages.

(G) The proportions of labeled adult HSCs (defined by the proportions of labeled KM myeloid lineages) in the three groups show significant differences. The subaortic AGM region-targeted group displays a significantly higher mean efficiency (12.8%) compared to the DA region-targeted group (1.35%) and the control (No HS) group (0.23%), with the highest labeling efficiency of around 60%. Data are presented as Mean ± SD. Welch's t test was used for significance calculations. **** $P<0.0001$.

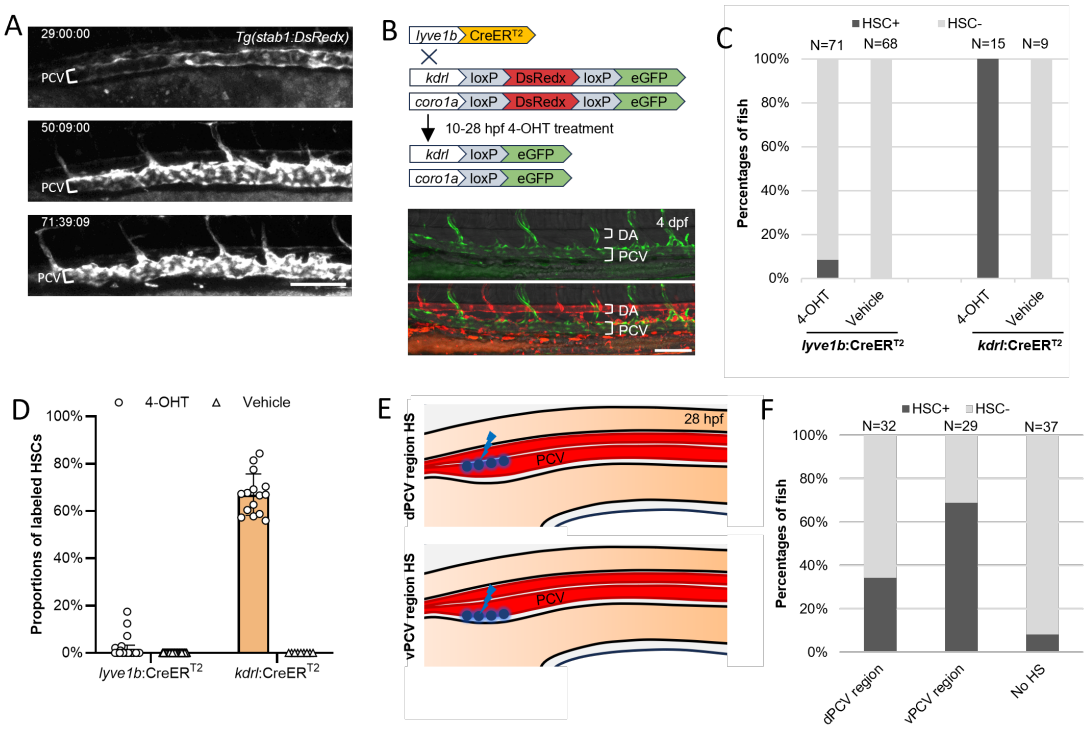

Figure 2. The posterior cardinal vein does not generate HSCs

(A) Representative images of time-lapse live imaging of anterior PCV during 29 hpf to 72 hpf in the *Tg(stab1:DsRedx)* fish. EHT-like events have not been detected in over 10 examined fish; only some autofluorescence-positive pigment cells are visible in the subvenous region.

(B-D) Venous vessel-specific lineage tracing denies the PCV as the origin of HSCs. The experimental principle is elucidated in the schematic diagram (B, upper panel). Fish were treated with 4-OHT from 10 hpf to 28 hpf, and labeling efficiency and specificity were confirmed by the eGFP^{+} vasculature pattern at 3 dpf using confocal microscopy (B, lower panel). Flow cytometry analysis of adult KM blood cells revealed that fewer than 9% of the *lyve1b*:CreER^{T2}-activated fish (6/71) showed eGFP^{+} blood cells in adult KM (C, left two columns), with an average of 0.61% HSC-labeling efficiency (D, left column). In contrast, all pan-vessel-specific *kdrl*:CreER^{T2}-activated fish (positive control) display eGFP^{+} blood cells in adult KM (C, right two columns), with an average of 66.97% HSC-labeling efficiency (D, right column). To ensure sufficient sample size for reliable percentages, the *lyve1b*:CreER^{T2}-mediated and *kdrl*:CreER^{T2}-mediated lineage tracing data combine results from 4 and 2 independent experiments, respectively.

(E-F) Multi-cell resolution IR-LEGO lineage tracing indicates that HSCs arise from unidentified precursors located beneath the PCV. The schematic draw indicates the positions (dorsal and ventral sides of the PCV) targeted by infrared light in *Tg(hsp70l:mCherry-T2A-CreER^{T2};kdrl:LRLG;coro1a:LRLG)* fish at ~28 hpf (E). Flow cytometry analysis of adult KM blood cells reveals a significant higher percentage of

935 HSC-labeled fish in the ventral PCV region-targeted group (vPCV) compared to the
936 dorsal PCV region-targeted group (dPCV) (F). The data represents a combination of
937 three independent experiments, ensuring sufficient sample size for reliable percentages.

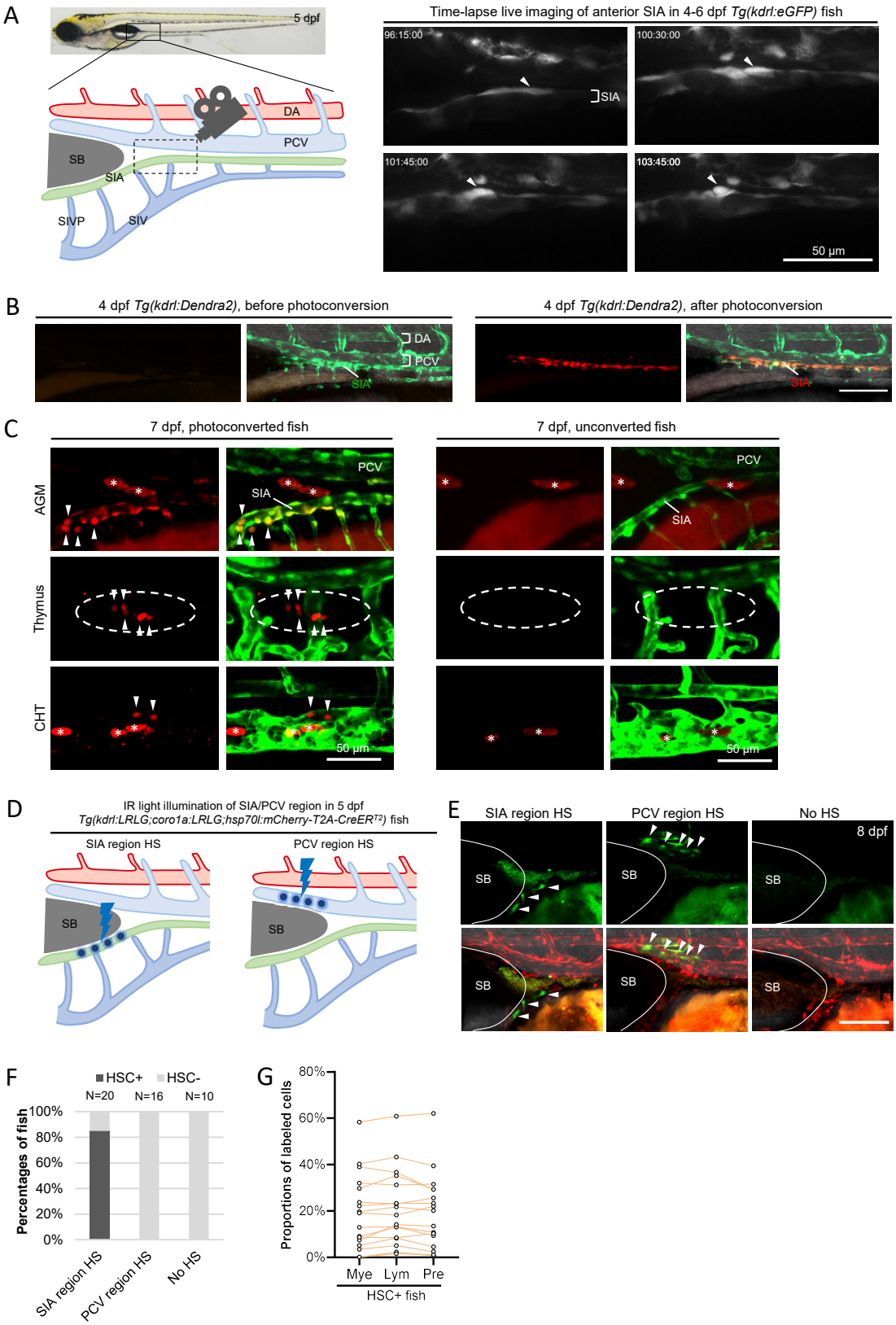

Figure 3. HSCs are generated from the supraintestinal artery via EHT

(A) Time-lapse live imaging of the subvenous vasculatures in 4 dpf to 6 dpf *Tg(kdrl:eGFP)* fish reveals EHT-like events in the SIA. The left panel depicts subvenous vasculature structures in the anterior AGM region, while the right panel

shows a representative EHT-like event (arrowhead) in the SIA, originating from the dashed line-boxed region in the left panel. SIA: supra-intestinal artery. SIV: sub-intestinal vein. SIVP: sub-intestinal venous plexus. SB: swimming bladder.

(B-C) Photoconversion-based transient lineage tracing reveals SIA-derived cells colonizing the thymus and CHT. Representative images of 4 dpf *Tg(kdrl:Dendra2)* fish indicate anterior SIA cells before and after the photoconversion (B). The photoconverted SIA cells give rise to hematopoietic cells-like descendants (arrowheads) that colonize the AGM, thymus (dished line circle), and CHT (C). Autofluorescence-positive pigment cells are marked by asterisks.

(D-G) The long-term lineage tracing using multi-cell resolution IR-LEGO cell labeling confirms the SIA as the origin of HSCs. The schematic diagram (D) indicates the anterior PCV region and SIA region targeted by infrared light in *Tg(hsp70l:mCherry-T2A-CreER^{T2};kdrl:LRLG;coro1a:LRLG)* zebrafish at 5 dpf. Labeling specificity was validated by eGFP^{+} vasculature pattern three days post-infrared light illumination (E). Flow cytometry analysis of the adult KM blood cells reveals successful HSC labeling in 85% SIA region-targeted fish (17 out of 20), whereas no labeling was observed in the PCV region-targeted group and No HS (control) fish (F). Adult blood cell-labeling efficiency, determined by assessing the proportions of labeled KM blood lineages (eGFP^{+} cells) in all KM blood cells (DsRedx^{+} + eGFP^{+} cells) in each HSC-labeled fish, is shown in panel G. The data represents a combination of three independent experiments to ensure sufficient sample size for reliable percentages.

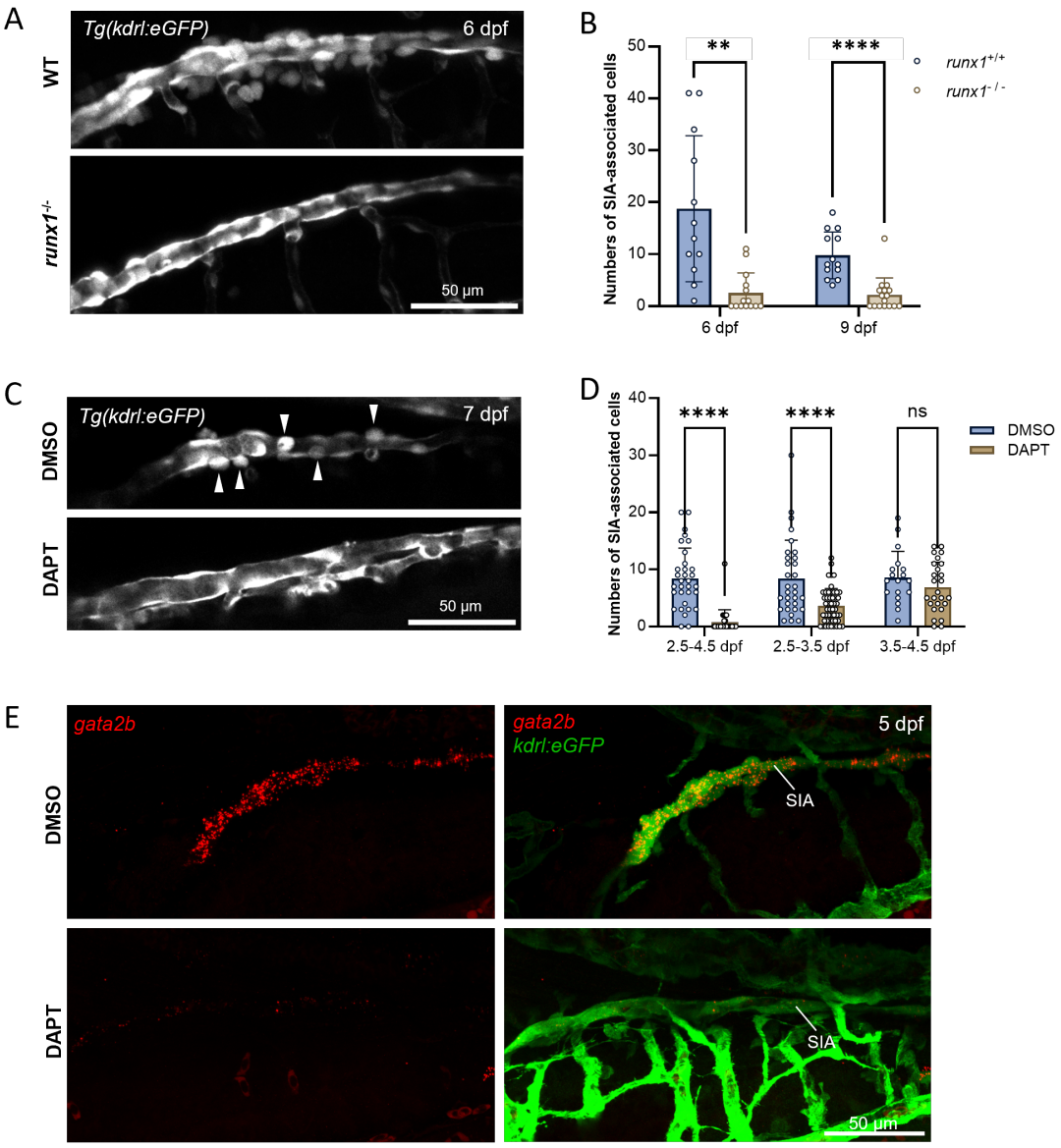

Figure 4. SIA hematopoiesis depends on *runx1* and Notch signaling

(A-B) SIA-associated HSPC-like cells are significantly reduced in *runx1*$^{-/-}$ *Tg(kdrl:eGFP)* fish. Data are presented as Mean ± SD. Welch's t test was utilized for significance calculations in 6 dpf samples, and Student's t-test was used for 9 dpf samples. ** P<0.01. **** P<0.0001.

(C-E) Notch inhibitor treatment blocks SIA hematopoiesis by suppressing HEC formation. Representative images and statistical data show SIA-associated HSPC-like cells (arrowheads) in 7 dpf DMSO-treated control fish, while these cells are largely absent in fish treated with DAPT from 2.5 dpf to 4.5 dpf (C, D). Additional DAPT treatment experiments confirm that Notch signaling is essential for SIA hematopoiesis before 3.5 dpf, prior to EHT onset (D), likely by disrupting HEC formation. The importance of Notch signaling is further supported by the lack of *gata2b* expression in the SIA, as shown by RNAscope in situ hybridization in 5 dpf *Tg(kdrl:eGFP)* fish treated with DAPT (from 2.5 dpf to 4.5 dpf) compared to the DMSO-treated controls

(E). Data are presented as Mean ± SD. Welch's t-test was used for significance calculations in the 2.5-4.5 dpf and 2.5-3.5 dpf treatment samples, while Student's t-test was employed for the 3.5-4.5 dpf treatment samples. **** $P<0.0001$. ns: non-significant.

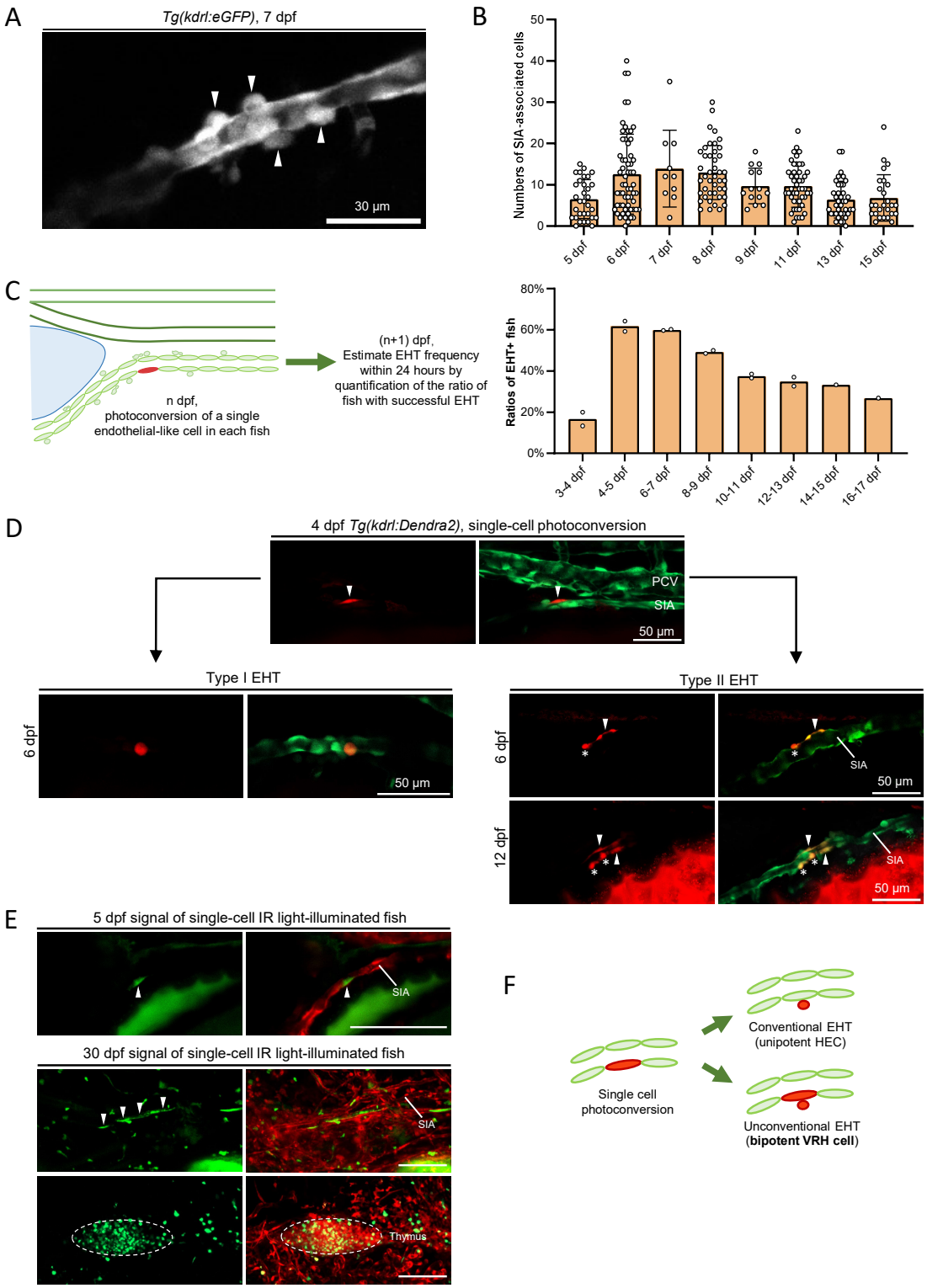

Figure 5. SIA hematopoiesis persists for at least two weeks through continuous cell division and budding of VRHs

(A-B) Characterization of SIA-associated nascent HSPC-like cells. A representative confocal microscopy image shows the SIA-associated nascent HSPC-like cells (arrowheads) (A). Quantification analysis reveals SIA-associated nascent HSPC-like cells persist from 5 dpf to at least 15 dpf (B).

(C) Single-cell photoconversion assay in the *Tg(kdrl:Dendra2)* fish unveils SIA EHT dynamics. The schematic diagram illustrates experimental processes, with EHT events evaluated 24 hours-post photoconversion. Quantification analysis shows that SIA EHT initiates at ~4 dpf, peaks at approximately 6 dpf, and gradually declines after 7 dpf.

(D) Short-term lineage tracing of photoconverted individual SIA cells identifies two EHT processes. In one process, photoconverted cells directly bud out from the SIA, producing only HSPC-like cells. In the other, photoconverted cells undergo multiple rounds of division and budding, generating both hematopoietic daughter cells (asterisks) and endothelial daughter cells that remain in the SIA (arrowheads) until at least 12 dpf. This observation suggests that the SIA contains both unipotent conventional HECs and bipotent precursors termed vessel resident hemangioblasts (VRHs).

(E) Long-term lineage tracing of infrared light-labeled individual SIA cells in *Tg(hsp70l:mCherry-T2A-CreER^{T2};fli1:LRLG;coro1a:LRLG)* zebrafish confirms the presence of VRHs. A successfully labeled single SIA cell (arrowhead) is shown in the upper panel. Subsequent tracing revealed abundant hematopoietic (including T lymphocytes in the thymus) and endothelial (arrowheads) descendants by 30 dpf (lower panels).

(F) Schematic summary of the two EHT types in the SIA.

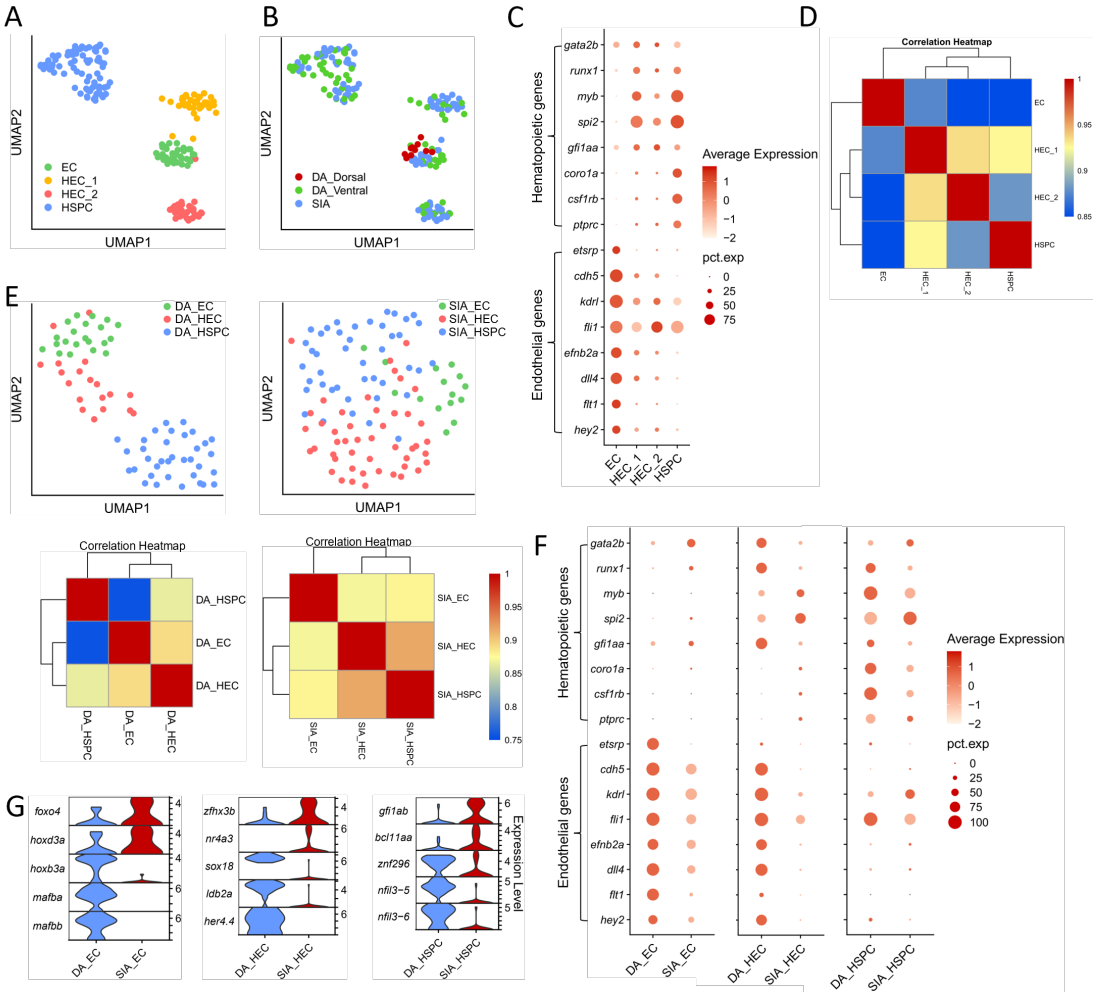

Figure 6. scRNA-seq supports the presence of VRHs and identifies potential regulators of SIA hematopoiesis

(A-B) UMAP analysis of 5 dpf SIA cells and 28 hpf DA cells reveals four distinct cell clusters (A) and their respective origins (B).

(C) Dot plot illustrates the expression patterns of selected hematopoietic and endothelial marker genes in the four clusters, defining their identities.

(D) Correlation heatmap reveals significant similarity between the HEC_1 and HEC_2 clusters.

(E) UMAP analysis (upper panel) and correlation analysis (lower panel) of DA and SIA clusters (HEC_1 and HEC_2 are merged as HEC) highlight their distinct characteristics: DA clusters are well-separated with lower correlation, while SIA clusters are largely intermingled with high correlation.

(F) Comparison of selected endothelial and hematopoietic marker expression in SIA and DA cells. DA ECs express strong endothelial markers but lack hematopoietic markers (left panel), while SIA ECs show weaker endothelial markers and express several notable hematopoietic markers like *gata2b*, *runx1*, and *gfi1aa* (left panel), supporting their bipotent nature. SIA HECs (middle panel) and SIA HSPCs (right panel)

exhibit distinct hematopoietic marker gene expression compared to DA counterparts, suggesting unique regulatory mechanisms in SIA hematopoiesis.

(G) Differential gene expression (DEG) analysis identifies distinct sets of transcription factors differentially expressed between SIA and DA cells.